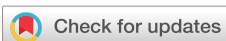


RESEARCH ARTICLE | NOVEMBER 06 2024

Symmetry breaker governs synchrony patterns in neuronal inspired networks

Anil Kumar  ; Edmilson Roque dos Santos  ; Paul J. Laurienti  ; Erik Boltt 

 Check for updates

Chaos 34, 113115 (2024)

<https://doi.org/10.1063/5.0209865>



Articles You May Be Interested In

Patterns of synchrony for feed-forward and auto-regulation feed-forward neural networks

Chaos (January 2017)

Regular synchrony lattices for product coupled cell networks

Chaos (January 2015)

Experimental investigations on the post-arc current of the vacuum circuit breaker in an active mechanical DC circuit breaker

AIP Advances (May 2021)

Symmetry breaker governs synchrony patterns in neuronal inspired networks

Cite as: Chaos 34, 113115 (2024); doi: [10.1063/5.0209865](https://doi.org/10.1063/5.0209865)

Submitted: 24 March 2024 · Accepted: 15 October 2024 ·

Published Online: 6 November 2024



View Online



Export Citation



CrossMark

Anil Kumar,^{1,2,a)} Edmilson Roque dos Santos,^{1,2,b)} Paul J. Laurienti,³ and Erik Boltt^{1,2}

AFFILIATIONS

¹Department of Electrical and Computer Engineering, Clarkson University, 8 Clarkson Ave., Potsdam 13699, New York, USA

²Clarkson Center for Complex Systems Science, Clarkson University, 8 Clarkson Ave., Potsdam 13699, New York, USA

³Department of Radiology, Wake Forest University School of Medicine, Medical Center Blvd, Winston-Salem 27101, North Carolina, USA

^{a)}Author to whom correspondence should be addressed: anikumar@clarkson.edu

^{b)}Also at: Instituto de Ciências Matemáticas e Computação, Universidade de São Paulo, São Carlos, Brazil.

ABSTRACT

Experiments in the human brain reveal switching between different activity patterns and functional network organization over time. Recently, multilayer modeling has been employed across multiple neurobiological levels (from spiking networks to brain regions) to unveil novel insights into the emergence and time evolution of synchrony patterns. We consider two layers with the top layer directly coupled to the bottom layer. When isolated, the bottom layer would remain in a specific stable pattern. However, in the presence of the top layer, the network exhibits spatiotemporal switching. The top layer in combination with the inter-layer coupling acts as a symmetry breaker, governing the bottom layer and restricting the number of allowed symmetry-induced patterns. This structure allows us to demonstrate the existence and stability of pattern states on the bottom layer, but most remarkably, it enables a simple mechanism for switching between patterns based on the unique symmetry-breaking role of the governing layer. We demonstrate that the symmetry breaker prevents complete synchronization in the bottom layer, a situation that would not be desirable in a normal functioning brain. We illustrate our findings using two layers of Hindmarsh–Rose (HR) oscillators, employing the Master Stability function approach in small networks to investigate the switching between patterns.

Published under an exclusive license by AIP Publishing. <https://doi.org/10.1063/5.0209865>

Experimental evidence in neuroscience indicates that the human brain exhibits diverse time-dependent synchrony patterns. Synchrony patterns refer to states in which certain brain regions exhibit coordinated activity while other regions do not, and these patterns can swiftly transition in response to external or internal stimuli. Inspired by this rapid switching phenomenon in the brain, we introduce a simple switching mechanism between synchrony patterns in networks. Since the brain is inherently heterogeneous, including different types of nerve cells, chemical compositions, various neuronal pathways, and intercellular interactions, incorporating heterogeneity among network components is crucial. Our work proposes a duplex network, where the bottom layer corresponds to the reference network to undergo transitions between synchrony patterns. We consider symmetry-induced synchrony patterns that are accessible by the bottom layer, so the top layer with inter-layer connections acts as a symmetry breaker governing the emerging symmetry-induced

patterns. The validity of the findings is tested through numerical simulations, assessing the linear stability of accessible invariant patterns. Our work highlights the significance of multilayer modeling in neuronal systems.

I. INTRODUCTION

Synchrony patterns in networks are found across different areas ranging from physics to neuroscience.^{1,2} Rather than exhibiting a fully synchronized cluster, networks often manifest diverse levels of synchronization throughout their structure. For instance, electroencephalogram (EEG) recorded data during unihemispheric sleep in some mammals and birds, in which one half of the brain is more active than the other, resembles distinct domains of synchronized elements.^{3,4} These synchrony patterns encompass synchronized nodes organized into different forms, including incoherent

states, chimera states, cluster states, and complete synchronous states. The specific pattern observed depends on the connectivity structure.^{2,5,6}

Experimental evidence in neuroscience suggests that synchrony patterns are spatiotemporal, evolving dynamically rather than remaining static.^{7–9} Neuroimaging experiments, spanning from functional MRI to EEG measurements of human brain activity, consistently reveal spatiotemporal patterns. Initial work on functional brain networks was primarily based on an assumption of network stationarity, but a large portion of current research examines dynamic changes in brain networks, even during the resting state.^{9–12} EEG data recorded during task performance also exhibit a mix of coordination dynamics characterized by both phase locking and metastability.⁸ Thus, consider a simplified toy example of a brain network depicted in Fig. 1(a), where the network transitions from one specific synchronized pattern to another. This scenario motivates a central question: How do these networks have the ability to switch between various synchrony patterns?

In the past few decades, significant effort has been dedicated to understanding synchrony patterns in networks, as evidenced by various studies.^{13–15} One well-established criterion to characterize such patterns is network symmetry.^{13,16} Symmetry refers to a permutation of nodes that leaves the network unchanged, preserving the neighbors of any two nodes that are permuted. The collection of all symmetries in a network forms an algebraic group, which, when applied to coupled identical units, gives rise to clusters. Clusters consist of equivalent nodes under the set of all symmetries, collectively forming a synchrony pattern in the network.⁵ Symmetry arguments are useful for characterizing synchrony patterns and their stability in networks of identical units.¹⁷ However, the brain contains billions of nerve cells, many different neurotransmitters, various neuronal pathways, and different types and strengths of interactions between the nerve cells.^{18,19} Therefore, incorporating heterogeneity among network components is crucial for a more accurate picture of switching between synchrony patterns in the brain.

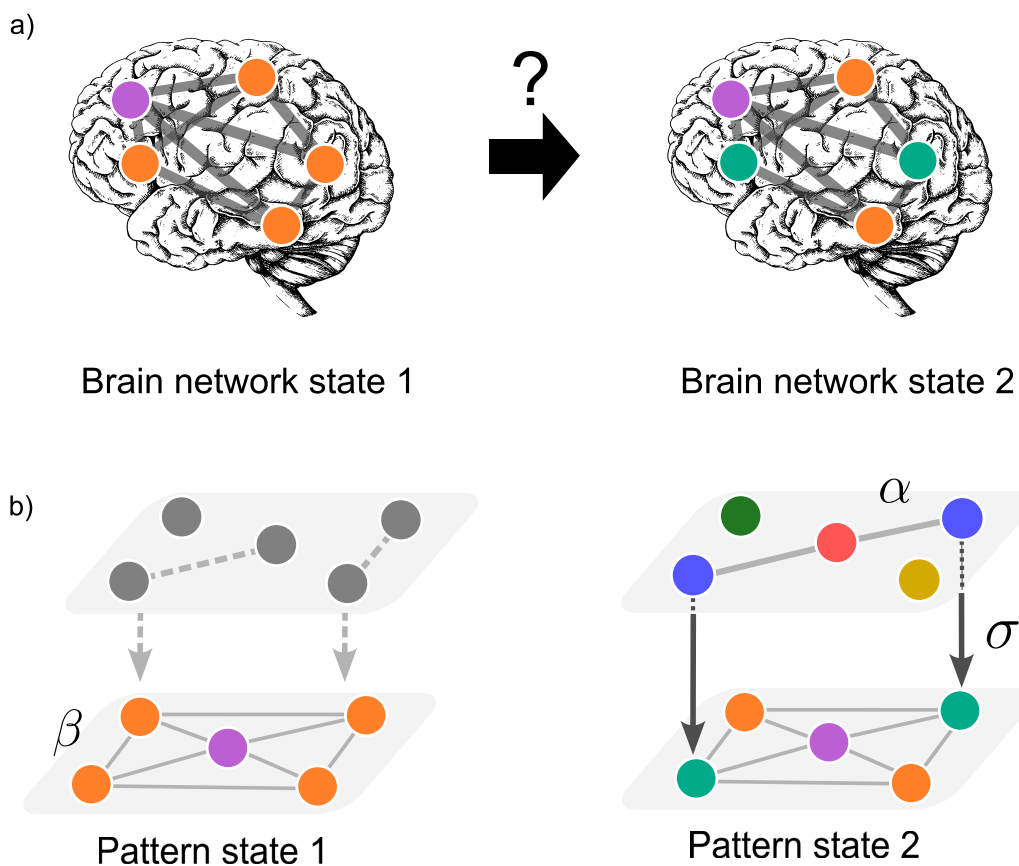


FIG. 1. Symmetry breaker underlies switching pattern states in neuronal networks. (a) Schematic diagram of the switching between brain network states. This represents our motivational toy example. (b) Each layer contains the same number of nodes, representing different instances of coupled units. Our focus is to observe the change of pattern in the bottom layer by the presence of the top layer and inter-layer connections, the symmetry breaker. The left panel shows the bottom layer exhibits the pattern state 1 for an intra-coupling β . The right panel shows that once the symmetry breaker is coupled to the bottom layer, the bottom layer shifts its state, exhibiting pattern state 2. Pattern state 1 leaves to be flow invariant, giving space to pattern state 2. The intra-layer α and inter-coupling σ are tuned to pinpoint pattern state 2's stability.

Multilayer modeling leverages different features of heterogeneous networks, where distinct node dynamics or coupling functions are considered layers of a multilayer network.²⁰ In neuroscience, multilayer modeling serves as a valuable tool for representing distinct information derived from the same set of entities and, in particular, this kind of model has been important specifically in applications to brain network.^{21–25} For instance, Crofts *et al.*²¹ investigated important structure–function relations in the Macaque cortical network by modeling it as a duplex network that comprises an anatomical layer, describing the known (macro-scale) network topology of the Macaque monkey, and a functional layer derived from simulated neural activity. Consequently, multilayer modeling has opened the possibility of addressing how neuronal networks switch between synchrony patterns.

Here, we propose a simple mechanism for switching between synchrony patterns in networks using two layers based on the symmetry-breaking role of a governing layer. We consider a network composed of two layers in which layers are named *top* and *bottom*. The bottom layer serves as the reference network and has several accessible symmetry-induced pattern states. When isolated, the bottom layer maintains a particular pattern state without temporal change. The switching between states emerges due to the presence of the top layer. The top layer and the inter-layer coupling constrains the symmetries of the bottom layer, determining which patterns are permissible—essentially acting as a *symmetry breaker*. We characterize the existence of symmetry-induced pattern states in a duplex network akin to.²⁶ Any bottom layer pattern exists if it remains flow invariant under permutation, taking the symmetry breaker into account. The stability of the patterns is assessed in terms of the Master Stability Function approach, which is simplified due to the directionality in inter-layer links. We illustrate the switching between pattern states using numerical simulations in coupled Hindmarsh–Rose oscillators with different node dynamics in each layer as well as different intra- and inter-layer coupling functions.

II. SYMMETRY BREAKER: MAPPING PATTERNS IN NETWORKS

We consider that each layer contains N nodes and the evolution of the system is given by

$$\begin{aligned}\dot{x}_i &= t(x_i) + \alpha \sum_{j=1}^N A_{ij} u(x_j), \\ \dot{y}_i &= b(y_i) - \beta \sum_{j=1}^N L_{ij} c(y_j) + \sigma \kappa_i D(x_i - y_i), \quad i = 1, 2, \dots, N,\end{aligned}\quad (1)$$

where $x_i, y_i \in \mathbb{R}^n$ are the state vectors of node i in top layer and bottom layer, respectively. We consider the following assumptions:

A. Isolated dynamics. We consider continuously differentiable top $t : \mathbb{R}^n \rightarrow \mathbb{R}^n$ and bottom $b : \mathbb{R}^n \rightarrow \mathbb{R}^n$ isolated dynamics, that have an inflowing invariant set, also referred to as dissipative systems. Most smooth nonlinear systems with compact attractors satisfy this assumption. For instance, Hindmarsh–Rose in Eq. (21) has an attractor.^{27,28}

B. Coupling function. The coupling functions $u, c : \mathbb{R}^n \rightarrow \mathbb{R}^n$ are continuously differentiable. The inter-coupling function is diffusive, depending on the difference of states, and $D \in \mathbb{R}^{n \times n}$.

C. Intra-layer coupling. The intra-coupling strength is given by α and β for the top layer and bottom layer, respectively. The intra-coupling structure of the top layer corresponds to adjacency matrix A , where the entries A_{ij} equal 1 if node i receives a connection from j and 0 otherwise. The intra-coupling of the bottom layer is given by a Laplacian matrix L . For both layers, the connectivity structure is undirected. So, the adjacency matrix and Laplacian matrix are symmetric and, consequently, have real eigenvalues.

D. Directed one-to-one but not onto inter-layer coupling. The symmetry of the whole multilayer structure moderates what pattern states are possible, and so changes between the layers allow the top layer to act as a governor over the bottom layer. We consider a non-symmetric inter-coupling between the two layers (unidirectionally) as illustrated in Fig. 1. The top layer drives the bottom layer through a one-to-one but not subjective coupling represented by the diagonal inter-layer matrix $K = \text{diag}(\kappa_1, \dots, \kappa_N) \in \mathbb{N}^{N \times N}$ (off-diagonal terms are zero) with each entry $\kappa_i \in \{0, 1\}$, and weighted by an overall inter-coupling strength σ . For instance, consider a 5×5 matrix

$$K = \begin{pmatrix} 1 & & & & \\ & 0 & & & \\ & & 1 & & \\ & & & 1 & \\ & & & & 0 \end{pmatrix}.$$

Our duplex setting is motivated by a recent work²⁹ on network reconstruction from the resting state functional MRI data from the National Consortium on Alcohol and NeuroDevelopment in Adolescence (NCANDA) study.³⁰ The study contrasted functional networks using two different network reconstruction methods, identifying that the networks have unique properties (with biological meaning) based on the method employed. Using Pearson correlation, one network corresponds to (near) synchronous functional relationships among brain regions, commonly employed in the neuroscience literature. The other network is constructed using optimal causation entropy,³¹ which identifies direct causal connections. The resulting network captures causal and nonlinear relations away from synchrony (if two nodes are synchronized, the causation entropy is zero), so it could be viewed as identifying asynchronous dynamics. The work indicates that analyzing both networks jointly provides a more comprehensive understanding of brain function, paving the way for a duplex modeling approach.

The above assumptions (A)–(D) qualitatively encode the different dynamical features of the two networks. The bottom layer—reference network—corresponds to (near) synchronization between brain regions, so we consider Laplacian intra-layer coupling that favors synchronization of nodes. As opposed to the top layer that captures asynchronous dynamics and can be modeled using the adjacency matrix as the intra-layer coupling, which does not favor synchronization among nodes. The coupling between both networks is the simplest inter-layer connectivity structure, a one-to-one coupling, allowing flexibility in the effective number of nodes influencing the bottom layer. We argue that these assumptions are

sufficient to induce the switching of patterns in the bottom layer caused by the top layer as described as follows.

Consider an initial state in the network of the five nodes, see the bottom left panel in Fig. 1. By the flow invariance, if the bottom layer starts at pattern state 1, it remains there and never shifts to pattern state 2. To allow the bottom layer to attain the other pattern state, we build up the idea of extending the phase space. We assume there exists a top layer, which evolves under different dynamics, coupled through an inter-layer connectivity structure. Out of all possible pattern states permitted in the bottom layer, only a subset is allowed due to symmetry constraints induced by the coupling with the top layer. We view the top layer and inter-layer coupling as a symmetry breaker that restricts, breaks, and changes symmetries on the bottom layer, see Fig. 1 for an illustration. To attain another pattern state, the symmetry breaker plays the role of mapping one pattern to another. Depending on the structural configuration of the top layer and inter-layer, the symmetry breaker shifts the initial pattern of the bottom layer to another state, which would be impossible in the absence of the symmetry breaker. Figure 1 illustrates the bottom layer switching from one pattern to another depending on the symmetry breaker structure.

The following sections are organized as follows. First, in Sec. III, it is shown that the topology of the bottom layer allows possible symmetry-induced clusters and, consequently, pattern states. Section IV is devoted to characterizing how the flow invariance of Eq. (1) and the structure of the symmetry breaker restrict symmetry-induced patterns in the bottom layer. Depending on the symmetry breaker structure, a particular pattern state can cease to exist due to a lack of flow invariance. Once the pattern state is flow invariant, the bottom layer attains this particular state whenever it is stable. Section V describes the linear stability of the full system (symmetry breaker and bottom layer). Section VI shows the numerical simulations in coupled Hindmarsh–Rose oscillators to demonstrate our findings. Section VII provides our discussion and conclusions.

Notation. Each vector $u_i \in \mathbb{R}^n$ is denoted $u_i = (u_i^1, \dots, u_i^n)$. The vector space \mathbb{R}^n is endowed with the ℓ_1 norm $\|u_i\|_1 = \sum_{k=1}^n |u_i^k|$. The state space $\mathbb{R}^n \otimes \mathbb{R}^N$ can be canonically identified with $(\mathbb{R}^n)^N$, which we will use for shorter notation. Each element of the space is $\mathbf{x} = \text{vec}(x_1, \dots, x_N) \in (\mathbb{R}^n)^N$, where vec denotes the vectorization by stacking multiple columns vectors into a single column vector. Also, $(\mathbb{R}^n)^N$ is equipped with the norm

$$\|\mathbf{x}\|_1 = \max_{i \in [N]} \|x_i\|_1.$$

Any linear operators on the above spaces will be equipped with the induced operator norm. Finally, let us denote I_n the $n \times n$ identity matrix in \mathbb{R}^n .

The notation for the state of the top and bottom layer can be recast as $\mathbf{x} = \text{vec}(x_1, \dots, x_N)$ and $\mathbf{y} = \text{vec}(y_1, \dots, y_N)$, respectively. Moreover, we introduce a tensor representation of Eq. (1) into a $2(Nn)$ -dimensional system. Define

$$\begin{aligned} \mathfrak{T}(\mathbf{x}) &= \text{vec}(\mathfrak{t}(x_1), \dots, \mathfrak{t}(x_N)), \\ \mathfrak{U}(\mathbf{x}) &= \text{vec}(\mathfrak{u}(x_1), \dots, \mathfrak{u}(x_N)), \\ \mathfrak{B}(\mathbf{y}) &= \text{vec}(\mathfrak{b}(y_1), \dots, \mathfrak{b}(y_N)), \\ \mathfrak{C}(\mathbf{y}) &= \text{vec}(\mathfrak{c}(y_1), \dots, \mathfrak{c}(y_N)). \end{aligned}$$

Then, Eq. (1) can be recast as

$$\dot{\mathbf{x}} = \mathfrak{T}(\mathbf{x}) + \alpha(A \otimes I_n)\mathfrak{U}(\mathbf{x}) \quad (2)$$

$$\dot{\mathbf{y}} = \mathfrak{B}(\mathbf{y}) - \beta(L \otimes I_n)\mathfrak{C}(\mathbf{y}) + \sigma(K \otimes D)(\mathbf{x} - \mathbf{y}), \quad (3)$$

where \otimes denotes the Kronecker product.

III. BOTTOM LAYER: SYMMETRY-INDUCED PATTERN STATES

Symmetries of a network are elements of the automorphism group of a graph, acting on the nodes of the network.³² Although symmetry is not a necessary condition for synchronization between nodes,¹³ it is sufficient for coupled identical oscillators.¹⁶ Then, we restrict ourselves to clusters, which are defined as groups of nodes that are synchronized to each other within the same group and distinct from other groups, induced by symmetries of the network, symmetry-based clusters.^{5,16} We will drop the term symmetry-based to characterize the clusters, but it should be clear that we are only dealing with those. More general mechanisms for inducing clusters such as balanced relation,^{13,14} external equitable partition (EEP),³³ and graph fibration³⁴ will be explored elsewhere.

To define cluster, we use orbit partition. The graph automorphism induces a partition of $[N] := \{1, \dots, N\}$.³² The collection of the graph automorphism orbits acting on $[N]$ induces the orbit partition of $[N]$:³⁵ $(\bigcup_{l=1}^{k_{\mathfrak{B}}} \mathcal{K}_{\mathfrak{B}}^l)$ such that $\mathcal{K}_{\mathfrak{B}}^l \cap \mathcal{K}_{\mathfrak{B}}^m = \emptyset$ for any $l \neq m \in [k_{\mathfrak{B}}]$, where $k_{\mathfrak{B}} \in \mathbb{N}$ is the number of clusters and $\mathcal{K}_{\mathfrak{B}}^l$ are the clusters. Nodes in $\mathcal{K}_{\mathfrak{B}}^l$ can be permuted among each other and will remain synchronized if started in a synchronized state. The trivial orbit partition consists of $\{\{1\}, \{2\}, \dots, \{N\}\}$.

From the orbit partition, we define the pattern state. Let $s_l \in \mathbb{R}^n$ be the state of the l th cluster. Then, the *pattern state* of the bottom layer is defined as

$$\mathcal{P}_{\mathfrak{B}} = \{\mathbf{y} \in \mathcal{V} \subset (\mathbb{R}^n)^N : y_i = s_l \in \mathbb{R}^n, \quad i \in \mathcal{K}_{\mathfrak{B}}^l, l \in [k_{\mathfrak{B}}]\} \quad (4)$$

and has dimension $nk_{\mathfrak{B}}$, where \mathcal{V} is an inflow invariant set. $\mathcal{P}_{\mathfrak{B}}$ corresponds to a manifold embedded in $(\mathbb{R}^n)^N$. Since any element of the graph automorphism permutes with the Laplacian matrix, the pattern state is an invariant manifold under the bottom layer dynamics, i.e., Eq. (1) with $\sigma = 0$.

The graph automorphism has subgroups that also generate different sets of clusters and, consequently, different pattern states.¹⁷ To completely characterize all possible pattern states of the bottom layer, we must enumerate the graph automorphism and its subgroups. We employ computational algebra methods/dedicated discrete algebra software³⁶ that generate the group automorphism and its subgroups of the bottom layer, as explored in Refs. 5, 17, and 26. Figure 2 displays different patterns that emerge in a network with five nodes. Each color identifies a different cluster $\mathcal{K}_{\mathfrak{B}}^l$ in the network.

IV. RESTRICTING SYMMETRY-INDUCED PATTERNS

To define a cluster for a duplex topology, dynamical information must be taken into account: the set of nodes from different layers evolve under different isolated dynamics, see Eq. (1). So, nodes from different layers are not allowed to be permuted between



FIG. 2. Symmetry-induced pattern states. Each orbit partition induced by the graph automorphism and its subgroups creates different patterns in the network with five nodes. Four patterns are illustrated where node color corresponds to a cluster.

each other. In this case, clusters do not result directly from the orbit partition induced by the graph automorphism of the duplex, but from a subgroup where symmetries of the duplex are built up of symmetries that only permute nodes of the same layer.²⁶ We adapt to our case the exposition in Ref. 26. Since our setting only contains two layers and the inter-layer is not one-to-one, this allows us to obtain specific (and stronger) results about the emerging patterns in the duplex system as discussed below.

Let $\mathcal{G}_{\mathfrak{T}}$ and $\mathcal{G}_{\mathfrak{B}}$ be the graph automorphisms of the top layer and bottom layer, respectively. An element of any of these sets can be represented by a permutation matrix written in a representation in $[N]$. We abuse notation, we only deal with the matrix representatives. Let $P_{\mathfrak{B}} \in \mathcal{G}_{\mathfrak{B}}$ be a permutation matrix that satisfies $P_{\mathfrak{B}} L = LP_{\mathfrak{B}}$. In order for Eq. (1) to be flow invariant under the action of this symmetry of the bottom layer, symmetry compatibility²⁶ must be achieved, which we state in our specialized scenario.

Proposition IV.1 (Symmetry compatibility²⁶). *Equation (1) is invariant under the action of $P_{\mathfrak{B}} \in \mathcal{G}_{\mathfrak{B}}$ if there exists $P_{\mathfrak{T}} \in \mathcal{G}_{\mathfrak{T}}$ such that the conjugacy relation*

$$P_{\mathfrak{B}} K = K P_{\mathfrak{T}} \quad (5)$$

is satisfied.

Proof. To achieve invariance of Eq. (1) under $P_{\mathfrak{B}} \in \mathcal{G}_{\mathfrak{B}}$, Eqs. (2) and (3) should be invariant under the action of $P_{\mathfrak{B}} \otimes I_n$. In fact, denote $\tilde{\mathbf{x}} = (P_{\mathfrak{T}} \otimes I_n)\mathbf{x}$ and $\tilde{\mathbf{y}} = (P_{\mathfrak{B}} \otimes I_n)\mathbf{y}$. We observe that the dynamics of $\tilde{\mathbf{x}}$ and $\tilde{\mathbf{y}}$ evolve as Eqs. (2) and (3), i.e., it is invariant, as long as given $P_{\mathfrak{B}}$ there exists $P_{\mathfrak{T}} \in \mathcal{G}_{\mathfrak{T}}$ such that the conjugacy relation is satisfied $P_{\mathfrak{B}} K = K P_{\mathfrak{T}}$. \square

The conjugacy relation constrains the possible symmetries of the bottom layer, depending on the topology of the top layer and inter-layer structure. The sets

$$\begin{aligned} \mathcal{H}_{\mathfrak{T}} &= \{P_{\mathfrak{T}} \in \mathcal{G}_{\mathfrak{T}} : \exists P_{\mathfrak{B}} \in \mathcal{G}_{\mathfrak{B}} \text{ s.t. } P_{\mathfrak{B}} K = K P_{\mathfrak{T}}\}, \\ \mathcal{H}_{\mathfrak{B}} &= \{P_{\mathfrak{B}} \in \mathcal{G}_{\mathfrak{B}} : \exists P_{\mathfrak{T}} \in \mathcal{G}_{\mathfrak{T}} \text{ s.t. } P_{\mathfrak{B}} K = K P_{\mathfrak{T}}\} \end{aligned} \quad (6)$$

are subgroups of $\mathcal{G}_{\mathfrak{T}}$ and $\mathcal{G}_{\mathfrak{B}}$, respectively. Since K is not a subjective map, the left and right null spaces are nontrivial. Consequently, we may find more than one $P_{\mathfrak{B}}$ that satisfies $P_{\mathfrak{B}} K = K P_{\mathfrak{T}}$ for a given $P_{\mathfrak{T}}$ and vice versa. Then, it is useful to define an equivalence relation between elements in $\mathcal{H}_{\mathfrak{T}}$, and similarly, in $\mathcal{H}_{\mathfrak{B}}$,

- $P_{\mathfrak{T}} \sim_r P'_{\mathfrak{T}}$ if the right multiplication is equal, $K P_{\mathfrak{T}} = K P'_{\mathfrak{T}}$;
- $P_{\mathfrak{B}} \sim_l P'_{\mathfrak{B}}$ if the left multiplication is equal, $P_{\mathfrak{B}} K = P'_{\mathfrak{B}} K$.

By the fundamental theorem on equivalence relations, these equivalence relations \sim_r and \sim_l define partitions $\mathcal{H}_{\mathfrak{T}}/\sim_r$ and $\mathcal{H}_{\mathfrak{B}}/\sim_l$ on $\mathcal{H}_{\mathfrak{T}}$ and $\mathcal{H}_{\mathfrak{B}}$, respectively. These partitions are the disjoint union of

a finite number of equivalence classes $\{\mathcal{E}_{\mathfrak{T}}^i\}_i$ and $\{\mathcal{E}_{\mathfrak{B}}^i\}_i$ as

$$\mathcal{H}_{\mathfrak{T}}/\sim_r = \bigcup_i \mathcal{E}_{\mathfrak{T}}^i \quad \mathcal{H}_{\mathfrak{B}}/\sim_l = \bigcup_i \mathcal{E}_{\mathfrak{B}}^i. \quad (7)$$

Then, the group of symmetries of the duplex is given by

$$\mathcal{G} = \left\{ \begin{pmatrix} P_{\mathfrak{T}} & 0 \\ 0 & P_{\mathfrak{B}} \end{pmatrix} \in \mathbb{R}^{2N \times 2N} : P_{\mathfrak{T}} \in \mathcal{E}_{\mathfrak{T}}^i, P_{\mathfrak{B}} \in \mathcal{E}_{\mathfrak{B}}^i \right\}. \quad (8)$$

Moreover, we also can define the clusters of the duplex network.

Definition IV.1 (Duplex clusters). Let \mathcal{G} be the symmetry group of the duplex. The collection of \mathcal{G} -orbits acting diagonally on $[N] \times [N]$ induces the orbit partitions $\{\mathcal{K}_{\mathfrak{T}}^j\}_{j=1}^{k_{\mathfrak{T}}}$ and $\{\mathcal{K}_{\mathfrak{B}}^l\}_{l=1}^{k_{\mathfrak{B}}}$ with $k_{\mathfrak{T}}$ and $k_{\mathfrak{B}}$ elements, respectively, that we call clusters of the top and bottom layers, respectively.

Note that $N = \sum_{l=1}^{k_{\mathfrak{B}}} |\mathcal{K}_{\mathfrak{B}}^l| = \sum_{l=1}^{k_{\mathfrak{B}}} |\mathcal{K}_{\mathfrak{B}}^l|$. Also, this definition leads to defining the pattern state of the duplex network. Let $r_j, s_k \in \mathbb{R}^n$ be the state of the j th cluster and k th cluster of the top and bottom layer, respectively. Then, the pattern state of the duplex network is defined as

$$\begin{aligned} \mathcal{P} = \{(\mathbf{x}, \mathbf{y}) \in \mathcal{U} \times \mathcal{V} \subset (\mathbb{R}^n)^N \times (\mathbb{R}^n)^N : x_i = r_j, y_j = s_k \in \mathbb{R}^n, \\ \times i \in \mathcal{K}_{\mathfrak{T}}^l, j \in \mathcal{K}_{\mathfrak{B}}^k, l \in [k_{\mathfrak{T}}], k \in [k_{\mathfrak{B}}]\} \end{aligned} \quad (9)$$

with dimension $d := n(k_{\mathfrak{T}} + k_{\mathfrak{B}})$, where \mathcal{U} and \mathcal{V} are inflow invariant sets. By construction, \mathcal{P} is an invariant manifold under Eq. (1). Note that from \mathcal{P} definition, it follows that in the absence of the symmetry breaker ($\sigma = 0$), projecting \mathcal{P} onto the second coordinates matches with the pattern state of the bottom layer $\mathcal{P}_{\mathfrak{B}}$ in Eq. (4), i.e., $\mathcal{P}_{\mathfrak{B}} = \pi_{\mathfrak{B}}(\mathcal{P})$, where $\pi_{\mathfrak{B}}$ is the canonical projection onto the coordinates of the bottom layer. Once the inter-coupling is positive, this does not necessarily hold, because the particular bottom layer pattern state $\mathcal{P}_{\mathfrak{B}}$ may not be invariant under the duplex dynamics in Eq. (1). The symmetry breaker does not only restrict the allowed symmetries of the bottom layer but also constraints on which pattern states are invariant under the duplex dynamics.

Given our specific setting, we also can state additional facts resulting from the invariance under the duplex dynamics.

Bottom layer clusters: all or nothing. The inter-layer structure is one-to-one (injective) but not onto (surjective). This particular structure implies further constraints on the bottom layer cluster in terms of a dichotomy:

- (i) Either the bottom layer cluster is not driven by any top layer cluster,
- (ii) or it receives one-to-one connections of a top layer cluster that has at least the same size.

See Corollary A.1 for the proof. This result also implies that $k_{\mathfrak{T}} \leq k_{\mathfrak{B}}$.

Symmetry breaker avoids complete synchronization. The bottom layer complete synchronous state is defined as $y_1 = y_2 = \dots = y_N = s$. In the absence of the symmetry breaker (when $\sigma = 0$), this state is an invariant state due to Laplacian coupling. Once the symmetry breaker is present, it loses the flow invariance for any inter-coupling strength $\sigma \neq 0$. In fact, the vector $\mathbf{1} = (1, 1, \dots, 1) \in \mathbb{R}^N$ is an eigenvector of L associated with the eigenvalue 0, $L\mathbf{1} = 0$. Hence, the intra-coupling term in the bottom layer dynamics Eq. (1) cancels out and only the inter-layer coupling remains. The bottom layer's complete synchronous state only remains invariant if two conditions are simultaneously satisfied: the top layer attains the complete synchronous state ($x_1 = x_2 = \dots = x_N$) and the inter-layer coupling matrix is $K = I_N$. Our assumptions violate both conditions; hence, the bottom layer's complete synchronous state is not invariant.

As aforementioned each layer can exhibit multiple admissible symmetry-induced pattern states, see Fig. 2. So, from here on we enumerate the pattern states using an additional index. The i th pattern state in the bottom layer is denoted as $\mathcal{P}_{\mathfrak{B}}^i$, similarly for the top layer or the duplex. Figure 3 displays eight distinct symmetry-induced patterns that emerge in the duplex network of each layer containing six nodes.

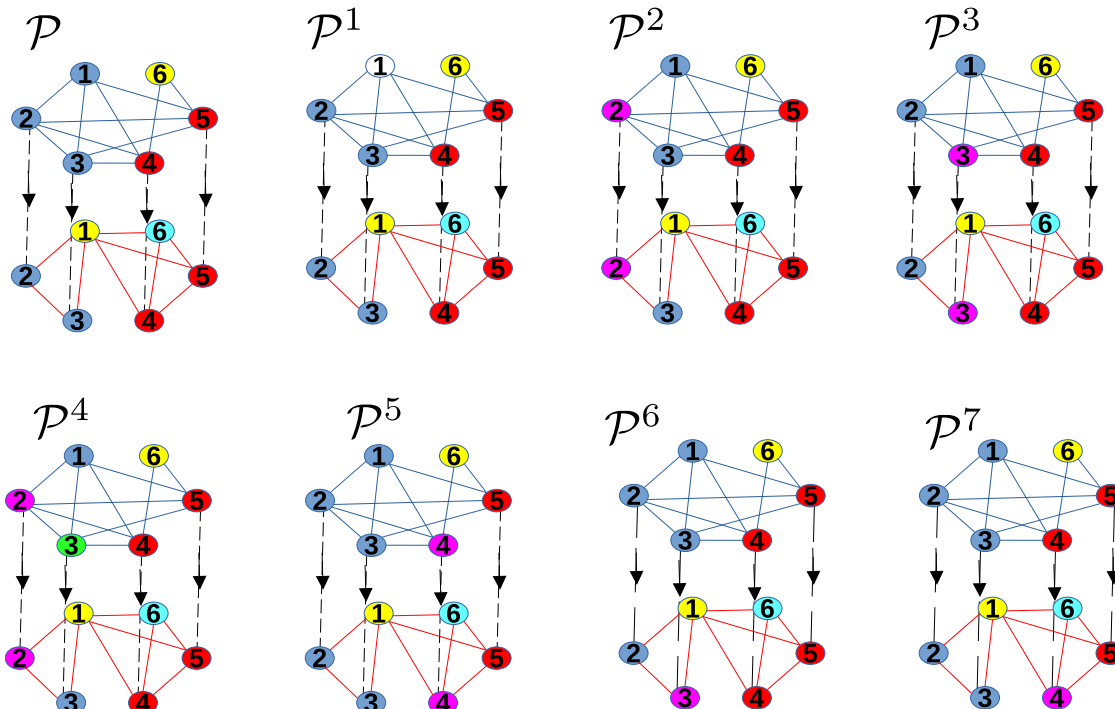


FIG. 3. Eight symmetry-induced pattern states in a duplex. Node colors denote the clusters of each layer. The top and bottom layers are illustrated using blue and red edges, respectively. The inter-layer connections are denoted as dashed directed edges. The construction of these patterns can be performed by breaking different synchronous clusters.³⁷ Pattern \mathcal{P} represents the pattern state constructed from the orbital partition of the group in Eq. (8) while $\mathcal{P}^1 - \mathcal{P}^7$ are patterns from breaking different synchronous clusters. $\mathcal{P}^1 - \mathcal{P}^4$ are generated from breaking $\mathcal{K}_{\mathfrak{T}}^1 = \{1, 2, 3\}$, \mathcal{P}^5 from $\mathcal{K}_{\mathfrak{T}}^2 = \{4, 5\}$, \mathcal{P}^6 from $\mathcal{K}_{\mathfrak{B}}^2 = \{2, 3\}$, and \mathcal{P}^7 from $\mathcal{K}_{\mathfrak{B}}^3 = \{4, 5\}$.

V. LINEAR STABILITY OF PATTERN STATES

Flow invariance under the duplex dynamics is a necessary condition so that the bottom layer may attain any particular pattern state. This leads to the question of when the pattern state is stable under a certain interval regime of the intra and inter-coupling strengths. In this section, we deduce the linear stability analysis for the duplex dynamics.

A. Pattern dynamics: Quotient dynamics

The dynamics on the pattern state \mathcal{P} of the duplex network lies in a reduced phase space with dimension $n(k_{\mathfrak{T}} + k_{\mathfrak{B}})$, where $k_{\mathfrak{T}}$ and $k_{\mathfrak{B}}$ are the number of clusters in the network. To obtain the equations of motion, also called quotient dynamics, we use the notation in Refs. 33 and 38 to characterize clusters and orbit partition.

We introduce the notation for the bottom layer, but use the same notation for the top layer, replacing the subscript by \mathfrak{T} . Let $e_{\mathfrak{B}}^l \in \mathbb{R}^N$ be given by the indicator vector that identifies the indices of the nodes in the l th cluster in the bottom layer, i.e.,

$$(e_{\mathfrak{B}}^l)_i = \begin{cases} 1, & i \in \mathcal{K}_{\mathfrak{B}}^l, \\ 0, & \text{otherwise.} \end{cases}$$

The orbit partition of $[N]$ into $k_{\mathfrak{B}}$ clusters is encoded in the characteristic matrix $E_{\mathfrak{B}} \in \mathbb{R}^{N \times k_{\mathfrak{B}}}$.³⁸ $E_{\mathfrak{B}}^{ij} = 1$ if node i belongs to cluster $\mathcal{K}_{\mathfrak{B}}^j$ and zero otherwise, i.e., the columns of $E_{\mathfrak{B}}$ are the indicator vectors $e_{\mathfrak{B}}^j$ of the clusters,

$$E_{\mathfrak{B}} = [e_{\mathfrak{B}}^1, \dots, e_{\mathfrak{B}}^{k_{\mathfrak{B}}}].$$

First note that $E_{\mathfrak{B}}^* E_{\mathfrak{B}}$ is invertible and diagonal with entries being the size of each cluster $\mathcal{K}_{\mathfrak{B}}^l$.³⁸ Also, let $\Pi_{\mathfrak{B}} \in \mathbb{R}^{N \times N}$ be defined

$$\Pi_{\mathfrak{B}} = E_{\mathfrak{B}} (E_{\mathfrak{B}}^* E_{\mathfrak{B}})^{-1} E_{\mathfrak{B}}^* = E_{\mathfrak{B}} E_{\mathfrak{B}}^+,$$

where $E_{\mathfrak{B}}^+$ is the left Moore–Penrose pseudoinverse of $E_{\mathfrak{B}}$ and can be seen as an average operator.³³ Then, $\Pi_{\mathfrak{B}}$ is symmetric, $\Pi_{\mathfrak{B}}^2 = \Pi_{\mathfrak{B}}$, and $\Pi_{\mathfrak{B}}$ and $E_{\mathfrak{B}}$ have the same column space. Hence, $\Pi_{\mathfrak{B}}$ represents the projection operator onto the column space of $E_{\mathfrak{B}}$, i.e., the subspace spanned by the vectors $\{e_{\mathfrak{B}}^l\}_{l=1}^{k_{\mathfrak{B}}}$. Moreover, $\Pi_{\mathfrak{B}}$ is block-diagonal with each diagonal block a multiple of the “all-ones” matrix.^{38,39} We denote the projection operator on the column space of $E_{\mathfrak{T}}$ and $E_{\mathfrak{B}}$ embedded into \mathbb{R}^{2N} as

$$\Pi = \begin{pmatrix} \Pi_{\mathfrak{T}} & 0 \\ 0 & \Pi_{\mathfrak{B}} \end{pmatrix}. \quad (10)$$

Denote $\mathbf{r} = \text{vec}(r_1, \dots, r_{k_{\mathfrak{T}}}) \in (\mathbb{R}^n)^{k_{\mathfrak{T}}}$ and $\mathbf{s} = \text{vec}(s_1, \dots, s_{k_{\mathfrak{B}}}) \in (\mathbb{R}^n)^{k_{\mathfrak{B}}}$. Then, the isolated dynamics and coupling function evaluated at the pattern state (\mathbf{r}, \mathbf{s}) of the duplex network are given by

$$\begin{aligned} \mathfrak{T}_{\mathbf{r}}(\mathbf{r}) &= \text{vec}(\mathfrak{t}(r_1), \dots, \mathfrak{t}(r_{k_{\mathfrak{T}}})) , \\ \mathfrak{U}_{\mathbf{r}}(\mathbf{r}) &= \text{vec}(\mathfrak{u}(r_1), \dots, \mathfrak{u}(r_{k_{\mathfrak{T}}})) , \\ \mathfrak{B}_{\mathbf{s}}(\mathbf{s}) &= \text{vec}(\mathfrak{b}(s_1), \dots, \mathfrak{b}(s_{k_{\mathfrak{B}}})) , \\ \mathfrak{C}_{\mathbf{s}}(\mathbf{s}) &= \text{vec}(\mathfrak{c}(s_1), \dots, \mathfrak{c}(s_{k_{\mathfrak{B}}})) , \end{aligned}$$

and satisfy

$$\begin{aligned} \mathfrak{T}((E_{\mathfrak{T}} \otimes I_n)\mathbf{r}) &= (E_{\mathfrak{T}} \otimes I_n)\mathfrak{T}_{\mathbf{r}}(\mathbf{r}) \\ \mathfrak{U}((E_{\mathfrak{T}} \otimes I_n)\mathbf{r}) &= (E_{\mathfrak{T}} \otimes I_n)\mathfrak{U}_{\mathbf{r}}(\mathbf{r}) \\ \mathfrak{B}((E_{\mathfrak{B}} \otimes I_n)\mathbf{s}) &= (E_{\mathfrak{B}} \otimes I_n)\mathfrak{B}_{\mathbf{s}}(\mathbf{s}) \\ \mathfrak{C}((E_{\mathfrak{B}} \otimes I_n)\mathbf{s}) &= (E_{\mathfrak{B}} \otimes I_n)\mathfrak{C}_{\mathbf{s}}(\mathbf{s}). \end{aligned} \quad (11)$$

To obtain the quotient dynamics, we set $\mathbf{x} = (E_{\mathfrak{T}} \otimes I_n)\mathbf{r}$ and $\mathbf{y} = (E_{\mathfrak{B}} \otimes I_n)\mathbf{s}$ and replace in Eqs. (2) and (3). To recast as a reduced system, we introduce new matrices that are the quotient versions of A , L , and K , i.e., satisfy the following relations:

$$\begin{aligned} AE_{\mathfrak{T}} &= E_{\mathfrak{T}} A_{\mathbf{r}}, & LE_{\mathfrak{B}} &= E_{\mathfrak{B}} L_{\mathbf{s}}, \\ KE_{\mathfrak{T}} &= E_{\mathfrak{B}} K_{\mathbf{r}}, & KE_{\mathfrak{B}} &= E_{\mathfrak{B}} K_{\mathbf{s}}. \end{aligned}$$

The new matrices are given by

$$\begin{aligned} A_{\mathbf{r}} &= E_{\mathfrak{T}}^+ A E_{\mathfrak{T}} \in \mathbb{R}^{k_{\mathfrak{T}} \times k_{\mathfrak{T}}}, \\ L_{\mathbf{s}} &= E_{\mathfrak{B}}^+ L E_{\mathfrak{B}} \in \mathbb{R}^{k_{\mathfrak{B}} \times k_{\mathfrak{B}}}, \\ K_{\mathbf{r}} &= E_{\mathfrak{B}}^+ K E_{\mathfrak{T}} \in \mathbb{R}^{k_{\mathfrak{B}} \times k_{\mathfrak{T}}}, \\ K_{\mathbf{s}} &= E_{\mathfrak{B}}^+ K E_{\mathfrak{B}} \in \mathbb{R}^{k_{\mathfrak{B}} \times k_{\mathfrak{B}}}, \end{aligned} \quad (12)$$

where the one-to-one inter-layer structure $K = \text{diag}(\kappa_1, \dots, \kappa_N) \in \mathbb{N}^{N \times N}$ implies that $K_{\mathbf{r}}$ is a $k_{\mathfrak{B}} \times k_{\mathfrak{T}}$ matrix whose entries are

given by

$$K_{\mathbf{r}}^{ij} = \frac{1}{|\mathcal{K}_{\mathfrak{B}}^i|} \sum_{l \in \mathcal{K}_{\mathfrak{B}}^i \cap \mathcal{K}_{\mathfrak{T}}^j} \kappa_l,$$

and $K_s = \text{diag}\left(\frac{1}{|\mathcal{K}_{\mathfrak{B}}^1|} \sum_{l \in \mathcal{K}_{\mathfrak{B}}^1} \kappa_l, \dots, \frac{1}{|\mathcal{K}_{\mathfrak{B}}^{k_{\mathfrak{B}}}|} \sum_{l \in \mathcal{K}_{\mathfrak{B}}^{k_{\mathfrak{B}}}} \kappa_l\right)$, where $|\cdot|$ corresponds to the number of nodes belonging to the cluster.

As aforementioned, \mathcal{P} is an invariant manifold under the flow, using (11) the matrices in Eq. (12) we obtain the dynamics on \mathcal{P} as given by

$$\begin{aligned} \dot{\mathbf{r}} &= \mathfrak{T}_{\mathbf{r}}(\mathbf{r}) + \alpha(A_{\mathbf{r}} \otimes I_n)\mathfrak{U}_{\mathbf{r}}(\mathbf{r}), \\ \dot{\mathbf{s}} &= \mathfrak{B}_{\mathbf{s}}(\mathbf{s}) - \beta(L_{\mathbf{s}} \otimes I_n)\mathfrak{C}_{\mathbf{s}}(\mathbf{s}) + \sigma(K_{\mathbf{r}} \otimes D)\mathbf{r} - \sigma(K_s \otimes D)\mathbf{s}. \end{aligned} \quad (13)$$

Although invariance of the flow in Eq. (1) is sufficient to deduce the type of patterns allowed in the bottom layer, knowing if trajectories attain a particular pattern is another issue. It remains to show that there is contraction toward \mathcal{P} transversely. To this end, we obtain equations that govern the dynamics near \mathcal{P} . We adapt to our case the exposition in Ref. 40.

B. Linear flow close to the pattern state

In order to consider the stability of pattern states, we analyze small perturbations away from \mathcal{P} as

$$\begin{pmatrix} \mathbf{x} \\ \mathbf{y} \end{pmatrix} = \begin{pmatrix} E_{\mathfrak{T}} \otimes I_n & 0 \\ 0 & E_{\mathfrak{B}} \otimes I_n \end{pmatrix} \begin{pmatrix} \mathbf{r} \\ \mathbf{s} \end{pmatrix} + \xi. \quad (14)$$

The first term in the sum defines a coordinate on \mathcal{P} , and the second term ξ is viewed as a perturbation to the pattern state. The coordinate splitting in Eq. (14) is associated with a splitting of $(\mathbb{R}^n)^N \times (\mathbb{R}^n)^N$ as the direct sum of subspaces

$$(\mathbb{R}^n)^N \times (\mathbb{R}^n)^N = \mathcal{F} \oplus \mathcal{F}^\perp$$

with associated projections

$$\pi_{\mathcal{F}} : (\mathbb{R}^n)^N \times (\mathbb{R}^n)^N \rightarrow \mathcal{F} \quad \pi_{\mathcal{F}^\perp} : (\mathbb{R}^n)^N \times (\mathbb{R}^n)^N \rightarrow \mathcal{F}^\perp.$$

The subspaces $\mathcal{F}, \mathcal{F}^\perp \subset (\mathbb{R}^n)^N \times (\mathbb{R}^n)^N$ are determined by embeddings from $(\mathbb{R}^n)^d$ and $(\mathbb{R}^n)^{(2N-d)}$, respectively, induced by the duplex group of symmetries \mathcal{G} . In fact, \mathcal{F} has a representation in terms of the column space of $E_{\mathfrak{T}}$ and $E_{\mathfrak{B}}$, respectively. Both matrices encode the cluster information of each layer, and the orthogonal complement of their column space forms a representation of \mathcal{F}^\perp . More precisely, the following result is valid

Proposition V.1 (Block diagonalization of coupling matrices.). Consider A and L the adjacency and Laplacian matrices of Eq. (1), respectively. Let $\Pi_{\mathfrak{T}}$ and $\Pi_{\mathfrak{B}}$ be orthogonal projection operators onto column spaces associated with clusters in the top and bottom layer, respectively. Consider the set of orthonormal eigenvectors $\{v_{\mathfrak{T}}^i\}_{i \in [N]}$ and $\{v_{\mathfrak{B}}^i\}_{i \in [N]}$ of $\Pi_{\mathfrak{T}}$ and $\Pi_{\mathfrak{B}}$, respectively, and

denote

$$T_{\mathfrak{T}} = [v_{\mathfrak{T}}^1, \dots, v_{\mathfrak{T}}^N] \quad \text{and} \quad T_{\mathfrak{B}} = [v_{\mathfrak{B}}^1, \dots, v_{\mathfrak{B}}^N].$$

Then, $B = T_{\mathfrak{T}}^* A T_{\mathfrak{T}}$ and $M = T_{\mathfrak{B}}^* L T_{\mathfrak{B}}$ are block-diagonal and denoted as

$$B = \begin{pmatrix} B^{\parallel} & 0 \\ 0 & B^{\perp} \end{pmatrix} \quad \text{and} \quad M = \begin{pmatrix} M^{\parallel} & 0 \\ 0 & M^{\perp} \end{pmatrix} \quad (15)$$

with $B^{\parallel} \in \mathbb{R}^{k_{\mathfrak{T}} \times k_{\mathfrak{T}}}$, $B^{\perp} \in \mathbb{R}^{(N-k_{\mathfrak{T}}) \times (N-k_{\mathfrak{T}})}$, $M^{\parallel} \in \mathbb{R}^{k_{\mathfrak{B}} \times k_{\mathfrak{B}}}$ and $M^{\perp} \in \mathbb{R}^{(N-k_{\mathfrak{B}}) \times (N-k_{\mathfrak{B}})}$.

Proof. See Appendix A 2. \square

First, the above result yields a representation for \mathcal{F} and \mathcal{F}^{\perp} ,

$$\begin{aligned} \mathcal{F} &= \text{span} \left\{ v_{\mathfrak{T}}^1, \dots, v_{\mathfrak{T}}^{k_{\mathfrak{T}}}, v_{\mathfrak{B}}^1, \dots, v_{\mathfrak{B}}^{k_{\mathfrak{B}}} \right\} \otimes \mathbb{R}^n, \\ \mathcal{F}^{\perp} &= \text{span} \left\{ v_{\mathfrak{T}}^{k_{\mathfrak{T}}+1}, \dots, v_{\mathfrak{T}}^N, v_{\mathfrak{B}}^{k_{\mathfrak{B}}+1}, \dots, v_{\mathfrak{B}}^N \right\} \otimes \mathbb{R}^n. \end{aligned}$$

Second, the range of the adjacency matrix A and the Laplacian matrix L can be split into these two subspaces, i.e., it performs a block diagonalization and the blocks are denoted with \parallel and \perp symbols. Different approaches are also possible such as irreducible representations (IRR),⁵ cluster-based coordinates,⁴¹ and simultaneous block diagonalization (SBD).⁴²

Here, we consider a pattern state to be stable if the transversal perturbations decay exponentially to zero. To determine the linear stability of a pattern state, we study dynamics close to the pattern state. Let $F_{\mathfrak{B}}^l \in \mathbb{R}^{N \times N}$ for each $l \in [k_{\mathfrak{B}}]$ be defined as

$$F_{\mathfrak{B}}^l = \text{diag}(e_{\mathfrak{B}}^l), \quad (16)$$

where $\sum_{l=1}^{k_{\mathfrak{B}}} F_{\mathfrak{B}}^l = I_N$, and similarly for $F_{\mathfrak{T}}^l$. To obtain a linear stability analysis, it suffices the linear flow close to the pattern state given by

$$\begin{aligned} \dot{\xi}_{\mathfrak{T}} &= \left(\sum_{l=1}^{k_{\mathfrak{T}}} F_{\mathfrak{T}}^l \otimes D\mathfrak{T}(r_l) + \alpha A F_{\mathfrak{T}}^l \otimes D\mathfrak{U}(r_l) \right) \xi_{\mathfrak{T}} \\ \dot{\xi}_{\mathfrak{B}} &= \left(\sum_{l=1}^{k_{\mathfrak{B}}} (F_{\mathfrak{B}}^l \otimes D\mathfrak{B}(s_l) - \beta L F_{\mathfrak{B}}^l \otimes D\mathfrak{C}(s_l)) - \sigma (K \otimes D) \right) \xi_{\mathfrak{B}} \\ &\quad + \sigma (K \otimes D) \xi_{\mathfrak{T}}, \end{aligned}$$

written in the coordinates $(\xi_{\mathfrak{T}}, \xi_{\mathfrak{B}})$ along a curve $(\mathbf{r}(t), \mathbf{s}(t))$ of the quotient dynamics Eq. (13). To obtain a decomposition of the linear flow into the subspaces \mathcal{F} and \mathcal{F}^{\perp} , Proposition V.1 introduces a change of coordinates

$$\begin{pmatrix} \xi_{\mathfrak{T}} \\ \xi_{\mathfrak{B}} \end{pmatrix} \mapsto \begin{pmatrix} T_{\mathfrak{T}}^* \otimes I_n & 0 \\ 0 & T_{\mathfrak{B}}^* \otimes I_n \end{pmatrix} \begin{pmatrix} \xi_{\mathfrak{T}} \\ \xi_{\mathfrak{B}} \end{pmatrix}, \quad (17)$$

which we abuse notation and still denote by $(\xi_{\mathfrak{T}}, \xi_{\mathfrak{B}})$ that splits the perturbation $(\xi_{\mathfrak{T}}, \xi_{\mathfrak{B}})$ further into parallel and transversal directions

$$\begin{aligned} \dot{\xi}_{\mathfrak{T}} &= \left(\sum_{l=1}^{k_{\mathfrak{T}}} G_{\mathfrak{T}}^l \otimes D\mathfrak{T}(r_l) + \alpha B G_{\mathfrak{T}}^l \otimes D\mathfrak{U}(r_l) \right) \xi_{\mathfrak{T}}, \\ \dot{\xi}_{\mathfrak{B}} &= \left(\sum_{l=1}^{k_{\mathfrak{B}}} G_{\mathfrak{B}}^l \otimes D\mathfrak{B}(s_l) - \beta M G_{\mathfrak{B}}^l \otimes D\mathfrak{C}(s_l) \right) \xi_{\mathfrak{B}} \\ &\quad \times \sigma (K_{\mathfrak{T}} \otimes D) \xi_{\mathfrak{T}} - \sigma (K_{\mathfrak{B}} \otimes D) \xi_{\mathfrak{B}}, \end{aligned} \quad (18)$$

where $G_{\mathfrak{T}}^l = T_{\mathfrak{T}}^* F_{\mathfrak{T}}^l T_{\mathfrak{T}}$, $G_{\mathfrak{B}}^l = T_{\mathfrak{B}}^* F_{\mathfrak{B}}^l T_{\mathfrak{B}}$, $K_{\mathfrak{T}} = T_{\mathfrak{B}}^* K T_{\mathfrak{T}}$, and $K_{\mathfrak{B}} = T_{\mathfrak{B}}^* K T_{\mathfrak{B}}$.

The linear stability of any top layer pattern does not depend on the bottom layer dynamics, due to the directed coupling inter-layer structure. Hence, to determine if a duplex pattern is stable, the top layer pattern counterpart must be stable. For general intra-coupling functions in both layers and inter-coupling functions, this problem can be assessed numerically, restricting the analysis to the columns associated with the transversal directions of the pattern state, as we detail in Sec. V C.

Remark V.1 (Laplacian coupling case). In the case of Laplacian coupling in the top layer, obtaining a stability condition for the coupling strengths (α, β, σ) becomes a nontrivial task. For $\sigma = 0$, under specific intra-layer structure⁴³ and linear coupling functions (satisfying special spectral conditions⁴⁰), the patterns are composed of independent clusters, and their corresponding stability can be assessed independently as well. In particular, the transversal directions of the pattern state in Eq. (18) can be analyzed in terms of exponential dichotomy⁴⁰ or Milnor stability.⁴³ However, for $\sigma \neq 0$ in Eq. (18), the parallel and transversal perturbations are coupled to each other, requiring further splitting to separate them. This goes beyond the scope of this paper and will be considered in future work.

C. Master stability approach

To characterize the stability of all clusters composing a pattern, we view the duplex as a single network composed of nodes, which lie on distinct layers, as having different types. To find the new coordinate system in Eq. (17) numerically, we apply a method for obtaining an irreducible block representation via symmetry breaking of a cluster into smaller clusters.³⁷ This method is suitable for directed networks as in our case when compared to other methods.^{26,44} We numerically solve all transverse perturbations in Eq. (18), along with the quotient dynamics given in Eq. (13). The Lyapunov exponents are estimated,^{45,46} tracking exponents associated with each cluster composing a pattern state. We denote Λ the largest of all Lyapunov exponents of a cluster. The stability of a pattern state for the top or bottom layer is based on the sign values of the largest exponents corresponding to each nontrivial cluster composing the pattern state. See Appendix A 3 for further details of the stability characterization of pattern states in the case of a duplex composed of six nodes in each layer.

VI. NUMERICAL SIMULATIONS

In this section, we present numerical simulations illustrating the switching between pattern states through the symmetry breaker. Fixing the topology of the symmetry breaker and β value, we only vary the coupling strengths (α, σ) to induce the switching. The directed inter-layer connections from top to bottom [Eq. (1)] guarantee that the existence of a pattern state in the top layer depends only on α , whereas patterns in the bottom layer depend on all coupling strengths, i.e., α, β, σ . We focus primarily on small networks to have a simple exposition in illustrating all admissible patterns of the network. However, the switching mechanism is also valid for large networks.

A. Determination of a pattern state

We must introduce a measure to quantify when the layer has attained a particular pattern state. Let $\mathcal{K}_{\mathfrak{B}}^l$ be the l th cluster in the bottom layer in a pattern $\mathcal{P}_{\mathfrak{B}}$. To determine which synchronous pattern exists in the bottom layer, we measure the synchronization error of the pattern $\mathcal{P}_{\mathfrak{B}}$, given as

$$\epsilon_{\mathcal{P}_{\mathfrak{B}}}(t) = \frac{1}{k_{\mathfrak{B}}} \sum_{l \in [k_{\mathfrak{B}}]} \epsilon_{\mathcal{K}_{\mathfrak{B}}^l}(t), \quad (19)$$

where

$$\epsilon_{\mathcal{K}_{\mathfrak{B}}^l}(t) = \frac{1}{|\mathcal{K}_{\mathfrak{B}}^l|(|\mathcal{K}_{\mathfrak{B}}^l| - 1)} \sum_{i,j \in \mathcal{K}_{\mathfrak{B}}^l} \|y_i(t) - y_j(t)\|_1. \quad (20)$$

When $\epsilon_{\mathcal{P}_{\mathfrak{B}}}(t)$ is away from zero the pattern does not exist at time t , while $\epsilon_{\mathcal{P}_{\mathfrak{B}}}(t)$ close to zero shows that the layer attained $\mathcal{P}_{\mathfrak{B}}$. Note that Eq. (20) is only defined for nontrivial clusters since trivial clusters have $|\mathcal{K}_{\mathfrak{B}}^l| = 1$. Therefore, a pattern state is decided by calculating the synchronization errors for all nontrivial clusters in

it. Similarly, we can define the synchronization error for the pattern $\mathcal{P}_{\mathfrak{T}}$ in the top layer.

The definition of the synchronization error in Eq. (19) allows us to deduce the following observations:

- (i) In case the synchronization error is away from zero for all patterns that contain at least one nontrivial cluster, then the bottom layer is in the incoherent state, which we denote as $\mathcal{P}_{\mathfrak{B}}^0$.
- (ii) Consider two distinct patterns $\mathcal{P}_{\mathfrak{B}}^i$ and $\mathcal{P}_{\mathfrak{B}}^j$. Note that whenever $\epsilon_{\mathcal{P}_{\mathfrak{B}}^i}(t)$ is close to zero but $\epsilon_{\mathcal{P}_{\mathfrak{B}}^j}(t) \neq 0$ as $t \rightarrow \infty$, we say the bottom layer is in pattern state $\mathcal{P}_{\mathfrak{B}}^i$.
- (iii) If two or more clusters merge in a pattern state $\mathcal{P}_{\mathfrak{B}}^i$ as we go from $\mathcal{P}_{\mathfrak{B}}^j$ to $\mathcal{P}_{\mathfrak{B}}^i$ and if $\epsilon_{\mathcal{P}_{\mathfrak{B}}^i}$ and $\epsilon_{\mathcal{P}_{\mathfrak{B}}^j}$ are both close to zero, the bottom layer is in pattern $\mathcal{P}_{\mathfrak{B}}^i$. For instance, suppose that $\epsilon_{\mathcal{P}_{\mathfrak{B}}^3}(t) = \epsilon_{\mathcal{P}_{\mathfrak{B}}^4}(t) \rightarrow 0$ in Fig. 4(a), then network β is in pattern $\mathcal{P}_{\mathfrak{B}}^4$.

Note that the same information about a pattern state can be deduced by plotting $\epsilon_{\mathcal{K}_{\mathfrak{B}}^l}(t)$ for all nontrivial clusters $\mathcal{K}_{\mathfrak{B}}^l$ as well. For networks exhibiting a small number of pattern states, plotting all synchronization errors corresponding to each nontrivial pattern is a straightforward way to determine which pattern state the network has attained.

B. Hindmarsh-Rose oscillators and coupling functions

We focus our attention on a neurologically relevant dynamical system and consider Hindmarsh-Rose (HR) oscillators⁴⁷ as nodes in both layers. Previous research has shown the emergence of different pattern states in the dynamics of coupled HR oscillators, particularly chimera states that are of interest to this paper.^{48,49} Hence, by proposing this switching mechanism, it seems natural to consider this simplification of the brain dynamics, employing a single-neuron

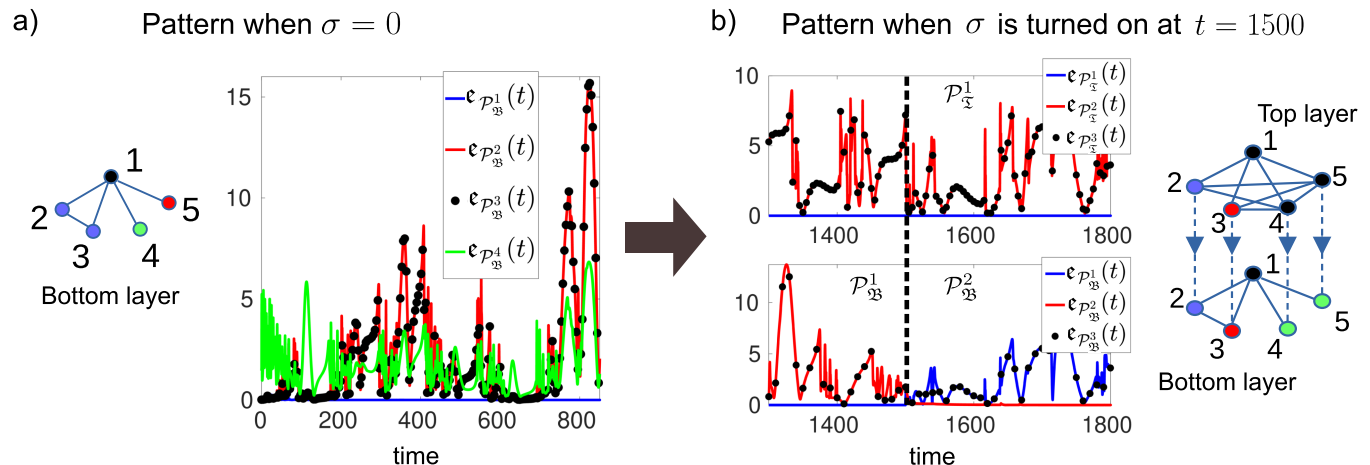


FIG. 4. Symmetry breaker governs pattern states in coupled HR oscillators. (a) Initially, when $\sigma = 0$, bottom layer is in one pattern state $\mathcal{P}_{\mathfrak{B}}^1 = \{(a, b, b, c, d)\}$. (b) The bottom layer switches to pattern $\mathcal{P}_{\mathfrak{B}}^2 = \{(a, b, c, d, d)\}$ in the presence of the symmetry breaker with $\alpha = 0.225$, when $\sigma = 0.5$ at $t = 1500$, represented by vertical dashed line. Node color corresponds to nodes in the same cluster, but the same color across layers has no meaning. The HR parameters are $I_{\mathfrak{T}} = 3.2$, $r_{\mathfrak{T}} = 0.01$, $I_{\mathfrak{B}} = 3.27$, $r_{\mathfrak{B}} = 0.01$, $\beta = 0.3$. The intra and inter-layer coupling functions are as shown in Eqs. (22) and (23).

model rather than large pools of neurons. Mesoscopic descriptions such as neural mass models^{50,51} and more elaborate models may also fit into our assumptions A and B in Sec. II, so this will be addressed for future research.

The bottom isolated dynamics b is given in arbitrary coordinates $(v, w, z) \in \mathbb{R}^3$ as

$$(v, w, z) \mapsto \begin{bmatrix} w - a_{\mathfrak{B}} v^3 + b_{\mathfrak{B}} v^2 - z + I_{\mathfrak{B}} \\ c_{\mathfrak{B}} - d_{\mathfrak{B}} v^2 - w \\ r_{\mathfrak{B}} (s_{\mathfrak{B}} [v - t_{\mathfrak{B}}] - z) \end{bmatrix}, \quad (21)$$

where $a_{\mathfrak{B}}, b_{\mathfrak{B}}, c_{\mathfrak{B}}, d_{\mathfrak{B}}, I_{\mathfrak{B}}, s_{\mathfrak{B}}$, and $t_{\mathfrak{B}}$ are parameters that determine the dynamical regime such as a fixed point, periodic orbit, or chaotic dynamics. We fix some of the parameters in Eq. (21) as $a_{\mathfrak{B}} = 1, b_{\mathfrak{B}} = 3, c_{\mathfrak{B}} = 1, d_{\mathfrak{B}} = 5, s_{\mathfrak{B}} = 4, t_{\mathfrak{B}} = -0.5(1 + \sqrt{5})$.⁴⁷ The isolated dynamics in the top layer t is the same as b , except that one or both parameters $I_{\mathfrak{T}} \neq I_{\mathfrak{B}}$ and $r_{\mathfrak{T}} \neq r_{\mathfrak{B}}$ are made different so that nodes in the layers are non-identical.

The intralayer coupling functions are as follows:

$$\mathbf{u}(x_j) = \begin{bmatrix} x_j^1 \\ 0 \\ 0 \end{bmatrix}, \quad \mathbf{c}(y_j) = \begin{bmatrix} y_j^1 \\ 0 \\ 0 \end{bmatrix}, \quad (22)$$

while the inter-layer coupling function follows the relation

$$D = \begin{bmatrix} 0 & 0 & 0 \\ 0 & 1 & 0 \\ 0 & 0 & 0 \end{bmatrix}. \quad (23)$$

Equation (1) is solved numerically using the Runge–Kutta fourth-order method with varying integration time steps. The solutions are discarded for some initial time interval so that the oscillators reach a steady state. To analyze any clusters $\mathcal{K}_{\mathfrak{T}}^l$ and $\mathcal{K}_{\mathfrak{B}}^m$ in the top and bottom layers, respectively, the initial conditions are selected such that $x_i(0) \approx x_j(0) \forall i, j \in \mathcal{K}_{\mathfrak{T}}^l$ and $y_i(0) \approx y_j(0) \forall i, j \in \mathcal{K}_{\mathfrak{B}}^m$.

C. Switching patterns states

Our numerical simulations show that the symmetry breaker can drive synchrony patterns in the bottom layer, using α and σ as control parameters. The switching between two patterns in the bottom layer can be described as follows: the desynchronization of a cluster in the top layer also breaks the corresponding compatible cluster in the bottom. Likewise, if a synchronized cluster exists in the top layer, increasing diffusive coupling through the y variable eventually synchronizes a compatible cluster in the bottom.⁵² Therefore, synchronization and desynchronization of clusters in the top layer change patterns at the bottom layer. Numerically, the switching is based on a time-dependent construction. First, the duplex system has time evolution characterized by a given pair of (α, σ) , exhibiting a particular pattern state in the bottom layer. After simulating the duplex system for some time, a new pair of (α, σ) is imposed, resulting in a different bottom layer pattern and, consequently, a switching.

Figure 4 displays the switching between pattern states in the bottom layer of five nodes. When the symmetry breaker is not present, $\sigma = 0$, the bottom layer is in pattern $\mathcal{P}_{\mathfrak{B}}^1 = \{(a, b, b, c, d)\}$ as shown by the time evolution of the synchronization error $\epsilon_{\mathcal{P}_{\mathfrak{B}}^1}(t)$

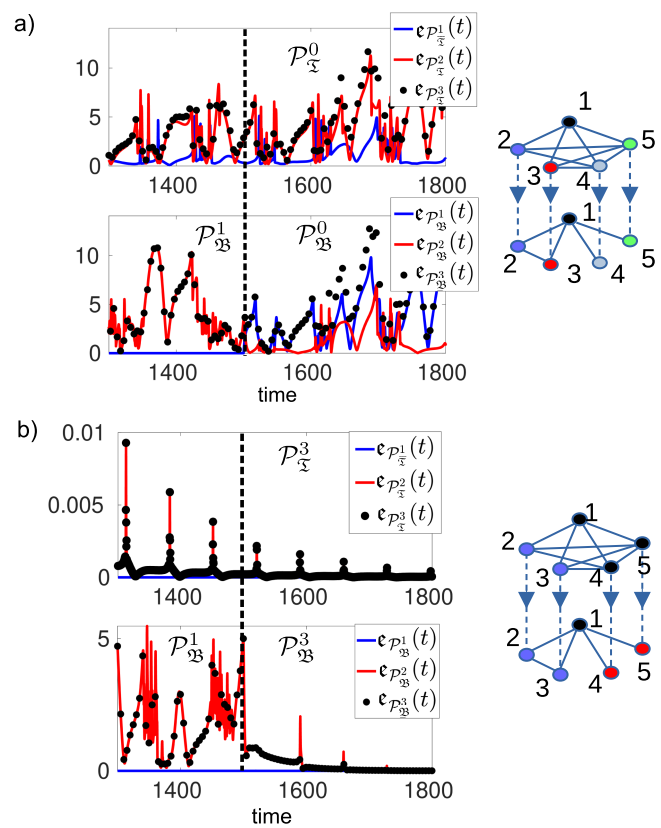


FIG. 5. Bottom layer can attain other patterns by changing α . (a) The bottom layer switches from $\mathcal{P}_{\mathfrak{B}}^1 = \{(a, b, c, d)\}$ to an incoherent pattern $\mathcal{P}_{\mathfrak{B}}^0 = \{(a, b, c, d, e)\}$ when $\alpha = 0.1$ and σ is turned on at $t = 1500$. (b) The bottom layer switches from $\mathcal{P}_{\mathfrak{B}}^1 = \{(a, b, b, c, d)\}$ to $\mathcal{P}_{\mathfrak{B}}^3 = \{(a, b, b, c, c)\}$ when $\alpha = 0.425$.

close to zero in Fig. 4(a) in comparison to the other admissible patterns such as $\mathcal{P}_{\mathfrak{B}}^2 = \{(a, b, c, d, d)\}$, $\mathcal{P}_{\mathfrak{B}}^3 = \{(a, b, b, c, c)\}$, and $\mathcal{P}_{\mathfrak{B}}^4 = \{(a, a, a, a, a)\}$. Then, for $\sigma \neq 0$ at $t = 1500$, we observe that the bottom layer switches from $\mathcal{P}_{\mathfrak{B}}^1$ to $\mathcal{P}_{\mathfrak{B}}^2$, as illustrated in Fig. 4(b). The synchronization error $\epsilon_{\mathcal{P}_{\mathfrak{B}}^1}(t)$ starts to oscillate away from zero, whereas $\epsilon_{\mathcal{P}_{\mathfrak{B}}^2}(t)$ decays to zero. To achieve this particular switching, the top layer attains the pattern state $\mathcal{P}_{\mathfrak{T}}^1 = \{(a, b, c, a, a)\}$ as quantified by the synchronization error $\epsilon_{\mathcal{P}_{\mathfrak{T}}^1}(t)$, which is constant and close to zero, illustrated in Fig. 4(b). The top layer or the symmetry breaker can exhibit nontrivial patterns $\mathcal{P}_{\mathfrak{T}}^1 = \{(a, b, c, a, a)\}$, $\mathcal{P}_{\mathfrak{T}}^2 = \{(a, b, b, c, d)\}$, and $\mathcal{P}_{\mathfrak{T}}^3 = \{(a, b, b, a, a)\}$. The initial conditions of each layer were selected such that the top and bottom layers were close to patterns $\mathcal{P}_{\mathfrak{T}}^3$ and $\mathcal{P}_{\mathfrak{B}}^3$, respectively. Choosing the same HR parameters and initial conditions from Fig. 4, but tuning α parameter, we can also observe that the bottom layer switches from the same pattern $\mathcal{P}_{\mathfrak{B}}^1$ to other patterns, see Fig. 5. In Fig. 5(a), the top layer is in the incoherent pattern, inducing that the bottom layer switches to the incoherent pattern $\mathcal{P}_{\mathfrak{B}}^0 = \{(a, b, c, d, e)\}$, as observed

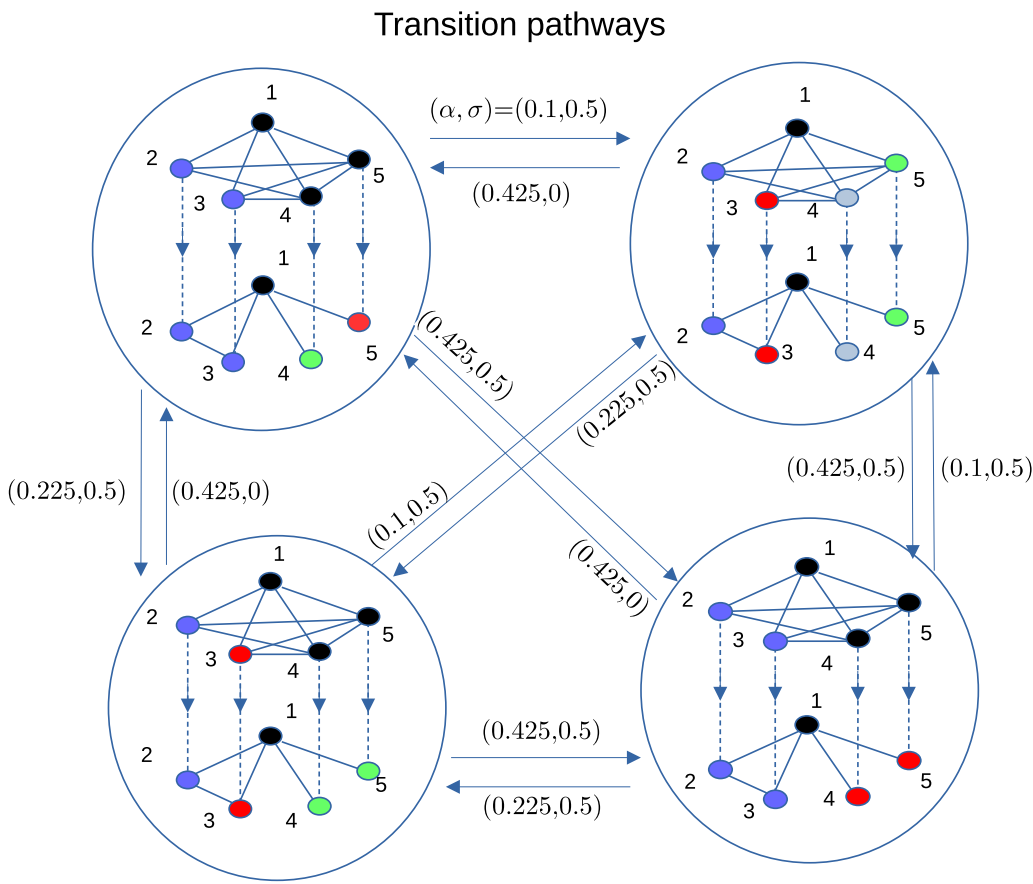


FIG. 6. Transition pathways driven by symmetry breaker. For a fixed symmetry breaker topology, regardless of the initial pattern state, the symmetry breaker drives the bottom layer to any other pattern state by choosing the appropriate pair of coupling strengths (α, σ) . There are total of four pattern states: $\mathcal{P}_{\mathfrak{B}}^1 = \{(a, b, b, c, d)\}$ (left top corner), $\mathcal{P}_{\mathfrak{B}}^2 = \{(a, b, c, d, e)\}$ (right top corner), $\mathcal{P}_{\mathfrak{B}}^3 = \{(a, b, b, c, c)\}$ (right bottom corner), and $\mathcal{P}_{\mathfrak{B}}^4 = \{(a, b, c, d, d)\}$ (left bottom corner). To draw these transition pathways, the numerical simulations have similar time-dependent construction and the same network dynamics parameters as in Fig. 4.

by all synchronization errors being away from zero after $t = 1500$. In Fig. 5(b), the bottom layer goes to $\mathcal{P}_{\mathfrak{B}}^3$, which contains the minimum number of symmetry-induced clusters, as illustrated by the synchronization errors of all patterns decaying to zero once σ is turned on.

All the switching phenomena occurred from the same pattern state, $\mathcal{P}_{\mathfrak{B}}^1$, and the bottom layer could attain any other pattern state apart from the complete synchronous pattern. In other words, from pattern $\mathcal{P}_{\mathfrak{B}}^1$ we found three possible transition pathways to other pattern states. But a natural question is: what are the admissible transition pathways starting from a different pattern? Figure 6 displays possible admissible transition pathways that switch the bottom layer's pattern, following the same time-dependent construction used in Figs. 4 and 5. Fixing the topology of the top layer and inter-coupling, the switching occurs only by changing (α, σ) . We observe that all transition pathways among pattern states form a complete directed graph, where the nodes are the pattern states, and the directed edges are the transition pathways. This confirms that the symmetry breaker can drive the bottom layer to a

different pattern state, regardless of which state the bottom layer starts at.

VII. DISCUSSION AND CONCLUSION

Building upon a multilayer perspective for neuronal network dynamics,^{6,53–57} the current work has proposed a mechanism for a network to switch between pattern states. The network is composed of two layers, a duplex network, where the bottom layer is the reference network. The top layer together with the inter-coupling connections forms a symmetry breaker, driving the invariant and stable symmetry-induced patterns in the bottom layer. Instead of characterizing the existence and stability of individual clusters,^{26,37,58,59} the relevant information is the collection of clusters that defines each symmetry-induced pattern. We have characterized all symmetry-induced pattern states in the bottom layer that are compatible in terms of the symmetry constraints imposed by the connections with the top layer. In particular, our work has demonstrated that the symmetry breaker avoids the complete synchronous state, which

corresponds to excessive (abnormal) synchrony and is associated with neurological disorders.⁶⁰ Although whole-brain synchrony is not desirable, clusters of synchronized regions that dynamically change membership and activity patterns, as shown here, likely underlie complex cognitive and emotional processes.^{7,61}

Our work has mapped the transition pathways of a set of admissible pattern states for small networks, fixing the symmetry breaker's topology. However, symmetry breakers are also capable of inducing specific and targeted symmetry-induced pattern states in networks. Hence, instead of fixing the topology, an interesting research direction is a control perspective:^{55,62} from a set of chosen symmetry-induced patterns in the bottom layer, to design the topology of the symmetry breaker such that the bottom layer can attain these particular pattern states. Although the inter-coupling connections are directed, which simplifies the analysis, similar results are also valid for bidirectional inter-coupling connections.

Our results show that the symmetry breaker governing the switching of patterns is a possible theoretical mechanism underlying the spatiotemporal synchrony patterns in the brain. The question is: how may this duplex network manifest in the brain? Motivated by recent work on network reconstruction from neuroimaging data,²⁹ instead of constructing a multilayer from structural vs functional data,^{21,22,25} our theoretical approach is flexible enough to support the following multilayer modeling: layers correspond to functional networks that are constructed using different techniques from the same observational data. The bottom layer represents the level of synchronization between brain regions, while the top layer represents the causal information flow between them. Each layer captures distinct features of neuronal dynamics within the same physical brain regions, offering complementary perspectives. In our model, we treat these different features as separate layer dynamics, each characterized by its own isolated dynamics, coupling functions, and topology. Since the nodes in both layers correspond to the same brain regions, the inter-layer connections follow a one-to-one coupling structure. Together, these layers form a multilayer network, providing a higher-dimensional description of the experimentally observed neuronal dynamics. This modeling approach highlights the potential of the symmetry breaker mechanism to stabilize different synchrony patterns through the interplay of the two layers. Overall, this mechanism can be added to the numerous possible dynamical mechanisms found in the literature: heteroclinic dynamics,⁶³ dynamics with riddled basins of attraction,⁶⁴ and multiple-timescale dynamics.⁶⁵ This opens the avenue for research to pinpoint the mechanism that better fits the observational data.

We also can hypothesize how this interplay between the top and bottom layers manifests via other forms in the brain. Multilayer modeling can match a hierarchical organization of the brain, where the top layer controls the bottom layer anatomically or functionally.^{66,67} This duplex structure is unlikely in a distributed system like the brain. It is also possible that the multilayer structure is analogical with all nodes in the same layer but having unique roles. Such an organization is much more likely in the brain with some nodes serving the symmetry breaker role and controlling the pattern states in other nodes. One could even imagine that this symmetry breaker role is dynamic with nodes flipping from the “top layer” to the “bottom layer” and vice versa depending on the state of the brain and the incoming sensory stimuli.

Our framework is strongly based on symmetry-induced patterns (and complete synchronization of trajectories) because there is a straightforward way to characterize the pattern states in terms of group actions on graphs. Moreover, for small networks, like the models used here, the pattern states of the bottom layer can be accessed numerically via the time evolution of the synchronization error (19). However, it is expected that brain networks do not possess exact symmetries. When building more neurobiological relevant models, one must characterize all admissible patterns, which is a nontrivial task for large networks. So, numerical techniques to identify different pattern states, allowing for approximate synchrony, via clustering⁶⁴ seem to be a promising direction. Our results will be explored in other network dynamics that include neurologically relevant information such as brain-inspired network topology and bio-physical details in the network dynamics. In summary, our work illustrates a mechanism by which one network can assist or drive patterns of synchrony in others, providing potential insights into switching between patterns in a complex system such as the brain.

ACKNOWLEDGMENTS

A.K., E.R.S., P.J.L., and E.B. acknowledge support from the Collaborative Research in Computational Neuroscience (CRCNS) through No. R01-AA029926. E.B. was also supported by ONR, ARO, DARPA RSDN, and AFSOR. E.R.S. was also supported by Serrapilheira Institute (Grant No. Serra-1709-16124). The brain graphic in Fig. 1 was extracted from FreePick.

AUTHOR DECLARATIONS

Conflict of Interest

The authors have no conflicts to disclose.

Author Contributions

Anil Kumar: Conceptualization (equal); Investigation (equal); Software (lead); Validation (equal); Visualization (equal); Writing – original draft (equal); Writing – review & editing (equal). **Edmilson Roque dos Santos:** Conceptualization (equal); Formal analysis (lead); Investigation (equal); Validation (equal); Visualization (equal); Writing – original draft (equal); Writing – review & editing (equal). **Paul J. Laurienti:** Funding acquisition (equal); Writing – review & editing (equal). **Erik Bullt:** Conceptualization (equal); Funding acquisition (equal); Investigation (equal); Methodology (lead); Supervision (lead); Writing – review & editing (equal).

DATA AVAILABILITY

The data that support the findings of this study are available from the corresponding author upon reasonable request.

APPENDIX A: BOTTOM LAYER'S CLUSTER: ALL OR NOTHING

The special choice of inter-coupling structure implies the following result:

Corollary A.1 (Bottom layer's cluster: all or nothing.). Consider a bottom layer cluster of size m . Then, one of the two scenarios holds

- (i) The bottom layer cluster does not receive connections at all.
- (ii) The bottom layer cluster receives one-to-one connections from a top layer cluster, which has at least the same size m .

The claim follows from the flow invariance of Eq. (1) and, consequently, from the symmetry compatibility IV.1.

Proof. Consider top and bottom layer clusters $\mathcal{K}_{\mathfrak{T}}$ and $\mathcal{K}_{\mathfrak{B}}$, respectively. Denote m as the size of the bottom layer cluster, i.e., $m = |\mathcal{K}_{\mathfrak{B}}|$. Let $K = \text{diag}(\kappa_1, \dots, \kappa_N)$ be the inter-layer coupling.

Note that if nodes i and j are in cluster $\mathcal{K}_{\mathfrak{B}}$, then there exists a permutation matrix $P_{\mathfrak{B}}$ that permutes these nodes and satisfies the symmetry compatibility in Eq. (5). So, there exists a permutation matrix $P_{\mathfrak{T}}$ that

$$KP_{\mathfrak{T}} = P_{\mathfrak{B}}K. \quad (\text{A1})$$

Also, note that $P_{\mathfrak{B}}$ permutes rows i and j of K . Since K is a diagonal matrix, to attain the Eq. (A1), $P_{\mathfrak{T}}$ must permute columns i and j of K . This implies that the entries of K satisfy $\kappa_i = \kappa_j$ for $i, j \in \mathcal{K}_{\mathfrak{T}}$. Repeating the argument to every node in the bottom layer $\mathcal{K}_{\mathfrak{B}}$, we obtain a constraint over the entries of K ,

$$\kappa_{i_1} = \kappa_{i_2} = \dots = \kappa_{i_m} = \begin{cases} 1, \\ 0 \end{cases}, \quad i_l \in \mathcal{K}_{\mathfrak{B}}.$$

Evaluating both cases implies the claim. \square

APPENDIX B: PROOF OF PROPOSITION V.1

Proof. We develop the proof for the Laplacian matrix, but the arguments can be repeated to the adjacency matrix. We split the proof into two steps.

Eigenspace of $\Pi_{\mathfrak{B}}$. $\Pi_{\mathfrak{B}}$ is an orthogonal projection operator onto the column space of $E_{\mathfrak{B}}$. Then, $\{e_{\mathfrak{B}}^l\}_{l=1}^{k_{\mathfrak{B}}}$ is the set of eigenvectors associated to the eigenvalue 1. So, denote $v_{\mathfrak{B}}^l = e_{\mathfrak{B}}^l$ for $l = 1, \dots, k_{\mathfrak{B}}$.

Consider the orthogonal complement of $\text{span}\{e_{\mathfrak{B}}^l\}_{l=1}^{k_{\mathfrak{B}}}$, where any vector is in the kernel of $\Pi_{\mathfrak{B}}$. To obtain a set of orthonormal eigenvectors $\{v_{\mathfrak{B}}^i\}_{i \in [N]}$ which diagonalizes $\Pi_{\mathfrak{B}}$, it suffices to extend the basis $\{v_{\mathfrak{B}}^l\}_l$ to a basis of \mathbb{R}^N and apply the Gram Schmidt process.

L and $\Pi_{\mathfrak{B}}$ commute. First, note that $\Pi_{\mathfrak{B}}$ is a doubly stochastic matrix. In fact, let $\mathbf{1}$ be the all ones vector, then $\Pi_{\mathfrak{B}}\mathbf{1} = \mathbf{1}$, and $\Pi_{\mathfrak{B}}$ is symmetric, so $\Pi_{\mathfrak{B}}$ is doubly stochastic. Using Birkhoff-von Neumann decomposition, $\Pi_{\mathfrak{B}}$ can be written as a convex combination of permutation matrices, i.e., there exist $c_1, \dots, c_d \in [0, 1]$ with $\sum_{p=1}^d c_p = 1$ and d different permutation matrices $P_{\mathfrak{B}}^1, \dots, P_{\mathfrak{B}}^d$ such that

$$\Pi_{\mathfrak{B}} = \sum_{p=1}^d c_p P_{\mathfrak{B}}^p. \quad (\text{B1})$$

For any node $i \in [N]$, if $\Pi_{\mathfrak{B}}^{ij} \neq 0$ then j belongs to the same cluster of i , i.e., a particular cluster $\mathcal{K}_{\mathfrak{B}}^i$. Since $\{\mathcal{K}_{\mathfrak{B}}^i\}_{i=1}^{k_{\mathfrak{B}}}$ is an orbit partition, then there exists at least one permutation matrix $P_{\mathfrak{B}}^p$ in the

decomposition (A2) that permutes i and j . Since the argument can be repeated for every node in the graph, we conclude that all permutation matrices $P_{\mathfrak{B}}^p$ are elements of one of the equivalence classes $\mathcal{E}_{\mathfrak{B}}^i$ and satisfy $P_{\mathfrak{B}}^p L = LP_{\mathfrak{B}}^p$. Then, $L\Pi_{\mathfrak{B}} = \Pi_{\mathfrak{B}} L$.

Since commuting matrices preserve eigenspaces, then L can be block-diagonalized using the set of eigenvectors of $\Pi_{\mathfrak{B}}$. Repeating the same sequence of arguments to the adjacency matrix, the proposition holds. \square

APPENDIX C: STABILITY CHARACTERIZATION FOR THE SWITCHING PHENOMENON

Here, we detail the stability characterization that underlies the switching phenomenon for an example of six nodes in the top and bottom layers, see Fig. 7. Figures 7(a) and 7(b) display the different patterns as we vary α and β while keeping $\sigma = 0$. To demonstrate the validity of our numerical simulations, we also plot the largest of all transverse Lyapunov exponents (Λ) associated with each nontrivial cluster along with numerical simulations. A side-by-side comparison between synchronization errors $\epsilon_{\mathcal{K}_{\mathfrak{T}}}^-(t)$ and $\epsilon_{\mathcal{K}_{\mathfrak{B}}}^-(t)$ for different clusters and the corresponding $\Lambda_{\mathcal{K}_{\mathfrak{T}}}$ and $\Lambda_{\mathcal{K}_{\mathfrak{B}}}$ values consolidate the accuracy of numerical simulations.

In Sec. IV, we discussed the effect on invariant synchronous clusters in the bottom network when it is connected with the top; invariant clusters whose corresponding permutation matrices do not satisfy the conjugacy relation, Eq. (5), are not invariant for any $\sigma > 0$. Therefore, the top layer restricts the number of identically synchronized clusters and, consequently, pattern states at the bottom layer. The first example is the complete synchronous state $\mathcal{P}_{\mathfrak{B}}^3 = \{(a, a, a, a, a, a)\}$, that exists for the bottom layer dynamics, confirmed by the synchronization error ϵ in the bottom panel of Fig. 7(b), but ceases whenever $\sigma > 0$, as explained in detail in Sec. IV. In addition, there are other two pattern states $\mathcal{P}_{\mathfrak{B}}^1 = \{(a, b, c, d, d, d)\}$ and $\mathcal{P}_{\mathfrak{B}}^2 = \{(a, b, b, c, c, c)\}$ which we focus here. The top panel of Fig. 7(b) shows the stability of the clusters, by tracing the maximum Lyapunov exponents, involved in these two particular pattern states. These patterns are not invariant for any $\sigma > 0$, or in other words, the corresponding permutation matrix $P_{\mathfrak{B}}$ does not have a $P_{\mathfrak{T}}$ in the top network that satisfies Eq. (5).

The top panel of Fig. 7(d) shows how the stability of bottom layers' patterns changes in the plane (α, σ) when driven by the top layer. The pattern $\mathcal{P}_{\mathfrak{B}}^0$ is stable at $\sigma = 0$, and increasing both α and σ , the patterns $\mathcal{P}_{\mathfrak{B}}^4$ and $\mathcal{P}_{\mathfrak{B}}^5$ become stable. If we separate the isolated dynamics from coupling terms in Eq. (18), the bottom panel of Fig. 7(d) shows the coupling matrix in the node space for the pattern state shown in Fig. 7(c). To obtain this coupling matrix, we have assumed that $\alpha = \beta = \sigma = 1$. The coupling matrix is such that B^\perp is decoupled from B^\parallel and M^\perp from M^\parallel . However, due to the one-way³⁷ inter-layer dependence of the bottom network on top, M^\perp is coupled with B^\perp , but the reverse is not true. Each row that is associated with B^\perp and M^\perp corresponds to a transverse perturbation that determines the stability of a cluster. Tracing all transverse Lyapunov exponents associated with a cluster with $|\mathcal{K}_{(\mathfrak{T})\mathfrak{B}}^l| > 2$ provides a detailed analysis about which nodes in an invariant cluster can synchronize at a given α and β .⁶⁸ For instance, for cluster $\mathcal{K}_{\mathfrak{T}}^1$, the coupling matrix shows that if $x_i(0) \approx x_j(0) \forall i, j \in \mathcal{K}_{\mathfrak{T}}^1$, all nodes in this cluster synchronize simultaneously.

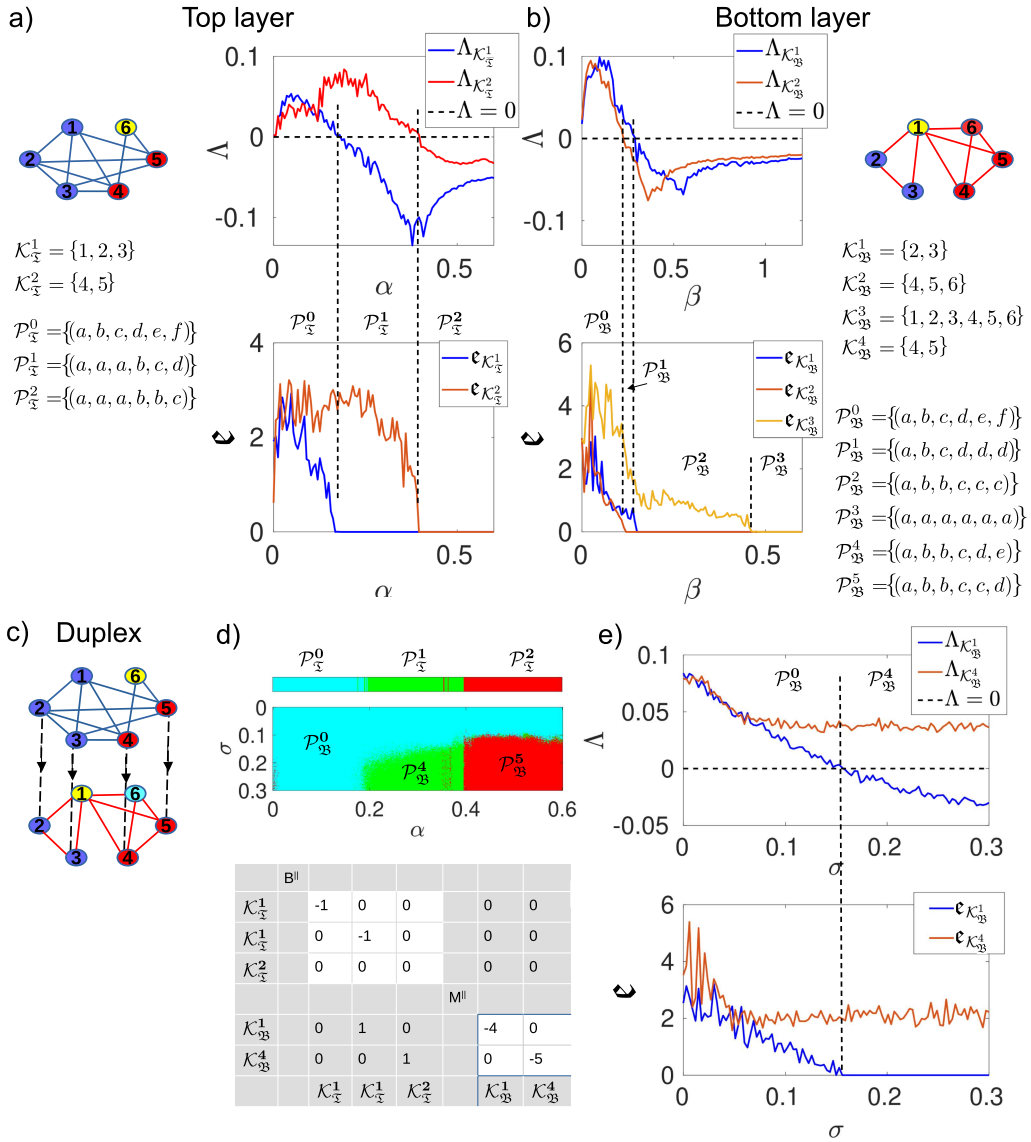


FIG. 7. Stability characterization for switching between patterns. (a) Pattern states in the top layer are depicted by the change in the largest Lyapunov exponent corresponding to each nontrivial cluster and a comparison with (time-averaged) synchronization errors from numerical simulations. (b) Pattern states in the bottom layer when $\sigma = 0$. (c) A multilayer network is constructed by joining the top and bottom layers through directed inter-layer links. (d) The top panel shows the stability analysis of the pattern states in the duplex network in (α, σ) space. The colors represent when the associated largest Lyapunov exponent is negative for a particular pattern. The bottom panel shows the transformed coupling matrix in the node space. (e) The stability analysis and (time-averaged) synchronization errors for compatible clusters in the bottom layer as σ changes. Here, we choose $\alpha = 0.2950$ (e) and $\beta = 0.05$ [(d) and (e)]. The HR parameters in all figures are $I_x = 3.1$, $r_x = 0.01$, $I_B = 3.2$, $r_B = 0.005$ and the coupling functions are given by Eqs. (22) and (23).

There are two types of synchronized clusters: independent and intertwined. Independent clusters are those whose existence does not require any other cluster to exist, i.e., they can exist independently, whereas intertwined clusters require all clusters (that are intertwined) to exist simultaneously. If any cluster in a set of

intertwined clusters desynchronizes, all intertwined clusters' stability is also lost. Using this fact, we have destabilized a synchronized cluster in the bottom layer. Such independence or dependence of clusters is visible from the coupling matrix in Fig. 7(d) as well, which shows that clusters $\mathcal{K}_x^1, \mathcal{K}_x^2$ are independent, while $\mathcal{K}_B^1, \mathcal{K}_B^4$ are

intertwined with $\mathcal{K}_{\mathfrak{T}}^1, \mathcal{K}_{\mathfrak{T}}^2$. While such intertwining of clusters is also possible within the bottom layer, our example contains intertwining across the layers only.

REFERENCES

- ¹A. Arenas, A. Díaz-Guilera, J. Kurths, Y. Moreno, and C. Zhou, "Synchronization in complex networks," *Phys. Rep.* **469**, 93–153 (2008).
- ²F. A. Rodrigues, T. K. D. Peron, P. Ji, and J. Kurths, "The Kuramoto model in complex networks," *Phys. Rep.* **610**, 1–98 (2016).
- ³M. J. Panaggio and D. M. Abrams, "Chimera states: Coexistence of coherence and incoherence in networks of coupled oscillators," *Nonlinearity* **28**, R67 (2015).
- ⁴Z. Wang and Z. Liu, "A brief review of chimera state in empirical brain networks," *Front. Physiol.* **11**, 724 (2020).
- ⁵L. M. Pecora, F. Sorrentino, A. M. Hagerstrom, T. E. Murphy, and R. Roy, "Cluster synchronization and isolated desynchronization in complex networks with symmetries," *Nat. Commun.* **5**, 4079 (2014).
- ⁶F. Parastesh, S. Jafari, H. Azarnoush, Z. Shahriari, Z. Wang, S. Boccaletti, and M. Perc, "Chimeras," *Phys. Rep.* **898**, 1–114 (2021).
- ⁷G. Buzsaki, *Rhythms of the Brain* (Oxford University Press, 2006).
- ⁸E. Tognoli and J. Kelso, "The metastable brain," *Neuron* **81**, 35–48 (2014).
- ⁹G. Deco, G. Tononi, M. Boly, and M. L. Kringelbach, "Rethinking segregation and integration: Contributions of whole-brain modelling," *Nat. Rev. Neurosci.* **16**, 430–439 (2015).
- ¹⁰D. A. Handwerker, V. Roopchansingh, J. Gonzalez-Castillo, and P. A. Bandettini, "Periodic changes in fMRI connectivity," *NeuroImage* **63**, 1712–1719 (2012).
- ¹¹C. Chang and G. H. Glover, "Time-frequency dynamics of resting-state brain connectivity measured with fMRI," *NeuroImage* **50**, 81–98 (2010).
- ¹²E. A. Allen, E. Damaraju, S. M. Plis, E. B. Erhardt, T. Eichele, and V. D. Calhoun, "Tracking whole-brain connectivity dynamics in the resting state," *Cereb. Cortex* **24**, 663–676 (2014).
- ¹³I. Stewart, M. Golubitsky, and M. Pivato, "Symmetry groupoids and patterns of synchrony in coupled cell networks," *SIAM J. Appl. Dyn. Syst.* **2**, 609–646 (2003).
- ¹⁴M. Golubitsky, I. Stewart, and A. Török, "Patterns of synchrony in coupled cell networks with multiple arrows," *SIAM J. Appl. Dyn. Syst.* **4**, 78–100 (2005).
- ¹⁵V. N. Belykh, G. V. Osipov, V. S. Petrov, J. A. K. Suykens, and J. Vandewalle, "Cluster synchronization in oscillatory networks," *Chaos* **18**, 037106 (2008).
- ¹⁶M. Golubitsky, *The Symmetry Perspective from Equilibrium to Chaos in Phase Space and Physical Space*, Progress in Mathematics Vol. 200 (Birkhäuser, Basel, 2002).
- ¹⁷F. Sorrentino, L. M. Pecora, A. M. Hagerstrom, T. E. Murphy, and R. Roy, "Complete characterization of the stability of cluster synchronization in complex dynamical networks," *Sci. Adv.* **2**, e1501737 (2016).
- ¹⁸C. Koch and G. Laurent, "Complexity and the nervous system," *Science* **284**, 96–98 (1999).
- ¹⁹E. Bullmore and O. Sporns, "Complex brain networks: Graph theoretical analysis of structural and functional systems," *Nat. Rev. Neurosci.* **10**, 186 (2009).
- ²⁰M. De Domenico, A. Solé-Ribalta, E. Cozzo, M. Kivelä, Y. Moreno, M. A. Porter, S. Gómez, and A. Arenas, "Mathematical formulation of multilayer networks," *Phys. Rev. X* **3**, 041022 (2013).
- ²¹J. J. Crofts, M. Forrester, and R. D. O'Dea, "Structure-function clustering in multiplex brain networks," *Europhys. Lett.* **116**, 18003 (2016).
- ²²M. De Domenico, "Multilayer modeling and analysis of human brain networks," *GigaScience* **6**, gix004 (2017).
- ²³F. Battiston, V. Nicosia, M. Chavez, and V. Latora, "Multilayer motif analysis of brain networks," *Chaos* **27**, 047404 (2017).
- ²⁴N. Frolov, V. Maksimenko, and A. Hramov, "Revealing a multiplex brain network through the analysis of recurrences," *Chaos* **30**, 121108 (2020).
- ²⁵M. Vaiana and S. F. Muldoon, "Multilayer brain networks," *J. Nonlinear Sci.* **30**, 2147–2169 (2020).
- ²⁶F. Della Rossa, L. Pecora, K. Blaha, A. Shirin, I. Klickstein, and F. Sorrentino, "Symmetries and cluster synchronization in multilayer networks," *Nat. Commun.* **11**, 3179 (2020).
- ²⁷V. Belykh, I. Belykh, and E. Mosekilde, "Hyperbolic Plykin attractor can exist in neuron models," *Int. J. Bifurcation Chaos* **15**, 3567–3578 (2005).
- ²⁸A. Shilnikov and M. Kolomiets, "Methods of the qualitative theory for the Hindmarsh–Rose model: A case study – a tutorial," *Int. J. Bifurcation Chaos* **18**, 2141–2168 (2008).
- ²⁹C. C. McIntyre, M. Bahrami, H. M. Shappell, R. G. Lyday, J. Fish, E. M. Boltt, and P. J. Laurienti, "Contrasting topologies of synchronous and asynchronous functional brain networks," bioRxiv 10.1101/2024.07.23.604765 (2024).
- ³⁰S. A. Brown, T. Brumback, K. Tomlinson, K. Cummins, W. K. Thompson, B. J. Nagel, M. D. De Bellis, S. R. Hooper, D. B. Clark, T. Chung, B. P. Hasler, I. M. Colrain, F. C. Baker, D. Prouty, A. Pfefferbaum, E. V. Sullivan, K. M. Pohl, T. Rohlfing, B. N. Nichols, W. Chu, and S. F. Tapert, "The National Consortium on Alcohol and Neurodevelopment in Adolescence (NCANDA): A multisite study of adolescent development and substance use," *J. Stud. Alcohol Drugs* **76**, 895–908 (2015).
- ³¹J. Sun, D. Taylor, and E. M. Boltt, "Causal network inference by optimal causation entropy," *SIAM J. Appl. Dyn. Syst.* **14**, 73–106 (2015).
- ³²F. Harary, *Graph Theory*, Addison-Wesley Series in Mathematics (Addison-Wesley Pub. Co, Reading, 1969).
- ³³M. T. Schaub, N. O'Clery, Y. N. Billeh, J.-C. Delvenne, R. Lambiotte, and M. Barahona, "Graph partitions and cluster synchronization in networks of oscillators," *Chaos* **26**, 094821 (2016).
- ³⁴L. DeVille and E. Lerman, "Modular dynamical systems on networks," *J. Eur. Math. Soc.* **017**, 2977–3013 (2015).
- ³⁵S. Kudose, see <https://www.math.uchicago.edu/may/VIGRE/VIGRE2009/REUPapers/Kudose.pdf> for "Equitable Partitions and Orbit Partitions."
- ³⁶W. Stein and D. Joyner, See <https://www.sagemath.org> for "SAGE: Software for Algebra and Geometry Experimentation" (2005).
- ³⁷M. Lodi, F. Sorrentino, and M. Storace, "One-way dependent clusters and stability of cluster synchronization in directed networks," *Nat. Commun.* **12**, 4073 (2021).
- ³⁸G. Hahn and G. Sabidussi, *Graph Symmetry*, Nato Science Series C: Mathematical and Physical Sciences Vol. 497 (Springer, Netherlands, 1997).
- ³⁹The network permutation matrix in Ref. 69.
- ⁴⁰T. Pereira, J. Eldering, M. Rasmussen, and A. Veneziani, "Towards a theory for diffusive coupling functions allowing persistent synchronization," *Nonlinearity* **27**, 501 (2014).
- ⁴¹Y. S. Cho, T. Nishikawa, and A. E. Motter, "Stable chimeras and independently synchronizable clusters," *Phys. Rev. Lett.* **119**, 084101 (2017).
- ⁴²Y. Zhang and A. E. Motter, "Symmetry-independent stability analysis of synchronization patterns," *SIAM Rev.* **62**, 817–836 (2020).
- ⁴³L. V. Gambuzza and M. Frasca, "A criterion for stability of cluster synchronization in networks with external equitable partitions," *Automatica* **100**, 212–218 (2019).
- ⁴⁴F. M. Brady, Y. Zhang, and A. E. Motter, "Forget partitions: Cluster synchronization in directed networks generate hierarchies," [arXiv:2106.13220\[nlin.AO\]](https://arxiv.org/abs/2106.13220) (2021).
- ⁴⁵J. P. Eckmann and D. Ruelle, "Ergodic theory of chaos and strange attractors," *Rev. Mod. Phys.* **57**, 617–656 (1985).
- ⁴⁶A. Pikovsky and A. Politi, *Lyapunov Exponents: A Tool to Explore Complex Dynamics* (Cambridge University Press, 2016).
- ⁴⁷J. L. Hindmarsh and R. M. Rose, "A model of neuronal bursting using three coupled first order differential equations," *Proc. R. Soc. London* **221**, 87–102 (1984).
- ⁴⁸J. Hizanidis, N. E. Kouvaris, G. Zamora-López, A. Díaz-Guilera, and C. G. Antonopoulos, "Chimera-like states in modular neural networks," *Sci. Rep.* **6**, 1–11 (2016).
- ⁴⁹S. Majhi, B. K. Bera, D. Ghosh, and M. Perc, "Chimera states in neuronal networks: A review," *Phys. Life Rev.* **28**, 100–121 (2019).
- ⁵⁰H. R. Wilson and J. D. Cowan, "Excitatory and inhibitory interactions in localized populations of model neurons," *Biophys. J.* **12**, 1–24 (1972).
- ⁵¹B. H. Jansen and V. G. Rit, "Electroencephalogram and visual evoked potential generation in a mathematical model of coupled cortical columns," *Biol. Cybern.* **73**, 357–366 (1995).
- ⁵²L. Huang, Q. Chen, Y.-C. Lai, and L. M. Pecora, "Generic behavior of master-stability functions in coupled nonlinear dynamical systems," *Phys. Rev. E* **80**, 036204 (2009).

- ⁵³S. Majhi, M. Perc, and D. Ghosh, "Chimera states in uncoupled neurons induced by a multilayer structure," *Sci. Rep.* **6**, 39033 (2016).
- ⁵⁴S. Majhi, M. Perc, and D. Ghosh, "Chimera states in a multilayer network of coupled and uncoupled neurons," *Chaos* **27**, 073109 (2017).
- ⁵⁵I. Omelchenko, T. Hülser, A. Zakharova, and E. Schöll, "Control of chimera states in multilayer networks," *Front. Appl. Math. Stat.* **4**, 67 (2019).
- ⁵⁶M. Mikhaylenko, L. Ramlow, S. Jalan, and A. Zakharova, "Weak multiplexing in neural networks: Switching between chimera and solitary states," *Chaos* **29**, 023122 (2019).
- ⁵⁷A. Zakharova, *Chimera Patterns in Networks* (Springer, 2020).
- ⁵⁸K. A. Blaha, K. Huang, F. Della Rossa, L. Pecora, M. Hosseini-Zadeh, and F. Sorrentino, "Cluster synchronization in multilayer networks: A fully analog experiment with LC oscillators with physically dissimilar coupling," *Phys. Rev. Lett.* **122**, 014101 (2019).
- ⁵⁹F. Sorrentino, L. Pecora, and L. Trajković, "Group consensus in multilayer networks," *IEEE Trans. Network Sci. Eng.* **7**, 2016–2026 (2020).
- ⁶⁰P. Jiruska, M. de Curtis, J. G. R. Jefferys, C. A. Schevon, S. J. Schiff, and K. Schindler, "Synchronization and desynchronization in epilepsy: Controversies and hypotheses," *J. Physiol.* **591**, 787–797 (2013).
- ⁶¹L. Pessoa, "Understanding brain networks and brain organization," *Phys. Life Rev.* **11**, 400–435 (2014).
- ⁶²L. V. Gambuzza, M. Frasca, F. Sorrentino, L. M. Pecora, and S. Boccaletti, "Controlling symmetries and clustered dynamics of complex networks," *IEEE Trans. Network Sci. Eng.* **8**, 282–293 (2021).
- ⁶³M. Morrison and L.-S. Young, "Chaotic heteroclinic networks as models of switching behavior in biological systems," *Chaos* **32**, 123102 (2022).
- ⁶⁴E. Boltt, J. Fish, A. Kumar, E. Roque dos Santos, and P. J. Laurienti, "Fractal basins as a mechanism for the nimble brain," *Sci. Rep.* **13**, 20860 (2023).
- ⁶⁵P. beim Graben, A. Jimenez-Marin, I. Diez, J. M. Cortes, M. Desroches, and S. Rodrigues, "Metastable resting state brain dynamics," *Front. Comput. Neurosci.* **13**, 62 (2019).
- ⁶⁶C. C. Hilgetag and A. Goulas, "'Hierarchy' in the organization of brain networks," *Philos. Trans. R. Soc. B: Biol. Sci.* **375**, 20190319 (2020).
- ⁶⁷G. Deco, D. Vidaurre, and M. L. Kringselbach, "Revisiting the global workspace orchestrating the hierarchical organization of the human brain," *Nat. Hum. Behav.* **5**, 497–511 (2021).
- ⁶⁸A. B. Siddique, L. Pecora, J. D. Hart, and F. Sorrentino, "Symmetry- and input-cluster synchronization in networks," *Phys. Rev. E* **97**, 042217 (2018).
- ⁶⁹W. Lin, H. Fan, Y. Wang, H. Ying, and X. Wang, "Controlling synchronous patterns in complex networks," *Phys. Rev. E* **93**, 042209 (2016).